Acta Pharmaceutica Sinica B 2025;15(3):1608−1625

Chinese Pharmaceutical Association
Institute of Materia Medica, Chinese Academy of Medical Sciences

Acta Pharmaceutica Sinica B

www.elsevier.com/locate/apsb
www.sciencedirect.com

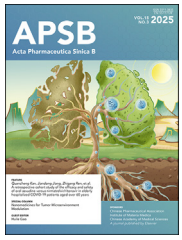

ORIGINAL ARTICLE

CDK5-triggered G6PD phosphorylation at threonine 91 facilitating redox homeostasis reveals a vulnerability in breast cancer

Yuncheng Bei[a,†], Sijie Wang[a,†], Rui Wang[a], Owais Ahmad[a], Meng Jia[b], Pengju Yao[c], Jianguo Ji[c,*], Pingping Shen[a,*]

[a]*Clinical Stem Cell Center, Nanjing Drum Tower Hospital, the Affiliated Hospital of Nanjing University Medical School and State Key Laboratory of Pharmaceutical Biotechnology, School of Life Sciences, Nanjing University, Nanjing 210023, China*
[b]*State Key Laboratory of Pharmaceutical Biotechnology, School of Life Sciences, Nanjing University, Nanjing 210023, China*
[c]*State Key Laboratory of Protein and Plant Gene Research, College of Life Sciences, Peking University, Beijing 100871, China*

Received 27 May 2024; received in revised form 9 July 2024; accepted 26 July 2024

KEY WORDS

Glucose-6-phosphoate dehydrogenase;
Pentose phosphate pathway;
CDK5;
Intracellular redox homeostasis;
Breast cancer;
Olaparib;
Drug resistance;
Isotopomer spectral analysis

Abstract Glucose-6-phosphate dehydrogenase (G6PD), the first rate-limiting enzyme of the pentose phosphate pathway (PPP), is aberrantly activated in multiple types of human cancers, governing the progression of tumor cells as well as the efficacy of anticancer therapy. Here, we discovered that cyclin-dependent kinase 5 (CDK5) rewired glucose metabolism from glycolysis to PPP in breast cancer (BC) cells by activating G6PD to keep intracellular redox homeostasis under oxidative stress. Mechanistically, CDK5-phosphorylated G6PD at Thr-91 facilitated the assembly of inactive monomers of G6PD into active dimers. More importantly, CDK5-induced pho-G6PD was explicitly observed specifically in tumor tissues in human BC specimens. Pharmacological inhibition of CDK5 remarkably abrogated G6PD phosphorylation, attenuated tumor growth and metastasis, and synergistically sensitized BC cells to poly-ADP-ribose polymerase (PARP) inhibitor Olaparib, in xenograft mouse models. Collectively, our results establish the crucial role of CDK5-mediated phosphorylation of G6PD in BC growth and metastasis and provide a therapeutic regimen for BC treatment.

*Corresponding authors.
E-mail addresses: jijg@pku.edu.cn (Jianguo Ji), ppshen@nju.edu.cn (Pingping Shen).
[†]These authors made equal contributions to this work.
Peer review under the responsibility of Chinese Pharmaceutical Association and Institute of Materia Medica, Chinese Academy of Medical Sciences.

https://doi.org/10.1016/j.apsb.2024.12.019

1. Introduction

Metabolic reprogramming is a major hallmark of human malignancies[1]. Due to the advancements in concepts over the past decade, the metabolic modifications that occur in cancer cells, such as converting glucose to lactate in the presence of oxygen (commonly referred to as the Warburg effect), have been thoroughly documented in cancer cells[1]. Reactive oxygen species (ROS), which are the byproducts of metabolic processes, accumulate in cancer cells during accelerated metabolism, hypoxia, or DNA damage. At high levels, these byproducts lead to biomolecular damage and even cell death. The maintenance of redox (reduction−oxidation) homeostasis through evolved, robust ROS-scavenging systems, partly *via* metabolism-mediated generation of reducing equivalents, promotes the malignant tumor progression and contributes to transient adaptive resistance or tolerance to cancer therapy[2-4].

The PPP diverges from glycolysis at the initial committed step, the dehydrogenation of glucose-6-phosphate (G6P), which has recently been identified as a crucial factor in cancer cell growth. G6P provides ribonucleotides and nicotinamide adenine dinucleotide phosphate (NADPH) for intracellular ROS detoxification, making it a critical component of cancer cell metabolism. Accumulated evidence has revealed a higher level of G6PD expression in various cancer tissues compared to paired normal tissues, with a strong correlation between G6PD expression and malignant development[3,5,6]. Moreover, overexpression of G6PD in non-malignant NIH 3T3 cells promotes anchorage-independent cell growth, which ultimately becomes tumorigenic and angiogenic in nude mice[7]. These findings imply that G6PD might be an independent prognostic predictor and a key target for therapeutic interventions against human malignancies. Indeed, inhibitors of G6PD activity, such as 6-aminonicotinamide (6-AN), dehydroepiandrosterone (DHEA), and polydatin, restrict the progression and metastasis of several human cancers, including prostate and mammary cancer[8-10].

Furthermore, impairing the antioxidant defense mechanisms of tumor cells *via* G6PD inhibition enhances their sensitivity to radiotherapy and chemotherapy as adjuvant treatments[11,12]. However, clinical trials of DHEA and 6-AN have been encumbered by the conversion of DHEA into active androgens and the on-target off-tumor toxicity of 6-AN[7]. Therefore, tumor-specific and enzyme-specific strategies to inhibit G6PD activity are urgently needed because of their potential to lead to the development of valuable therapies for cancer patients.

CDK5 is an atypical cyclin-dependent kinase (CDK) frequently overexpressed or hyperactivated in various cancer tissues and tumor cell lines[13]. Elevated CDK5 expression in tissues from patients with BC, brain cancer, and non-small cell lung cancer parallels advanced cancer stages, distant metastasis, and poor overall survival[14,15]. Our previous studies showed that CDK5 inhibition has therapeutic effects in BC. However, the molecular mechanisms underlying the CDK5 role in cancer progression remain poorly understood. In this study, we uncovered a novel association between CDK5 and G6PD in BC cells. Our findings indicate that CDK5 phosphorylates G6PD at Thr-91, which promotes the formation of active dimers from inactive monomers, thereby shifting BC cell glucose metabolism from the glycolytic pathway to the PPP. This shift protects BC cells from oxidative stress caused by glucose deprivation, anoikis, and ROS-based anticancer treatments. Therefore, CDK5-mediated G6PD phosphorylation may represent a promising therapeutic target for BC.

2. Materials and methods

2.1. Cell lines and cell culture

Human cell lines (non-malignant cell lines: 293T, and Huvec; non-small cell lung cancer cell line: A549; BC cell lines: MCF-7, MDA-MB-453 and MDA-MB-231; gastric cancer cell lines: NuGC4, MKN-45 and HGC27; melanoma cell line: A375; hepatocellular carcinoma cell line: HepG2; pancreatic cancer cell line: Panc-1) were originally purchased from the typical cell culture collection of the Committee of the Chinese Academy of Sciences Library and were cultured in RPMI-1640 medium (Invitrogen) or DMEM (Dulbecco's Modified Eagle's Medium) (Invitrogen) supplemented with 10% FBS (Bioind) and 1% penicillin−streptomycin at 37 °C with 5% CO_2 according to the supplier's instructions. Glucose-free RPMI-1640 medium (Thermo Fisher Scientific, cat. No. 11879020) was added with different concentrations of glucose and supplemented with 10% dialyzed FBS (ThermoFisher Scientific, cat. No. 26400-044) for the glucose deprivation assays. All cells tested negative for mycoplasma and were authenticated by short tandem repeat DNA fingerprinting at the Key Laboratory of Pharmaceutical Biotechnology and The Comprehensive Cancer Center of Nanjing University (Nanjing, China). All cell lines were not being passaged for more than 6 months in our study after resuscitation.

2.2. Isotopologue Spectral Analysis (ISA)

ISA quantified glucose metabolic flux. 1,2-$^{13}C_2$ glucose was purchased from Merck (cat. no. 453188) and used as the tracer as previously described[20]. Briefly, 10^7 cells exposed to the indicated treatments were grown for 24 h in RPMI-1640 with 10% FBS. Next, the media was exchanged for RPMI-1640 containing 10 μmol/L 1,2-$^{13}C_2$ glucose and 10% FBS, after which the cells were incubated for 24 h and harvested. Pre-cooled 80% (*v*/*v*) methanol was added to extract metabolites, followed by centrifugation at 14,000×*g* for 10 min at 4 °C. The supernatant was dried using a SpeadVac at room temperature. The dried supernatant was stored at −80 °C until the analysis. The extracts were reconstituted with 200 mL 50% (*v*/*v*) acetonitrile solution, vortexed for 5 min, and centrifuged at 14,000×*g* for 10 min at 4 °C. The supernatants were subjected to LC/MS analysis. The M+1/M+2 ratio indicates the ratio of glucose cycled through the oxidative PPP to glucose going directly through glycolysis.

2.3. Glucose uptake and lactate production

10^6 cells were transfected with the indicated overexpression vectors or incubated with inhibitors. The culture medium was changed for glucose consumption and lactate production, and the cells were incubated for an additional 24 h. Glucose levels were measured using a Glucose Colorimetric assay kit (Merck, cat. no. MAK181-1KT). Lactate levels were determined using a Lactate Assay Kit (Merck, cat. no. MAK064-1KT). The values were normalized to the total protein amount as determined using a BCA protein assay kit (Beyotime, cat. no. P0012S).

2.4. Vectors, site-directed mutagenesis, cell transfection, and lentivirus production

The lentiviral expression vector pLenti-CMV-EGFP-3Flag was purchased from OBIO. Full-length human *CDK1*, *CDK2*, *CDK5*, and *G6PD* were amplified and inserted into this vector. *G6PD-T91A*, *G6PD-T466A*, *G6PD-T91D*, *G6PD-T91E*, and *CDK5-D144N* mutated vectors were generated using a Muta-Direct Site-Directed Mutagenesis Kit (SBS Genetech Co., Ltd., China). The primers used in this study were as follows: *T91A* forward, 5′-CAAGGCCGCCCCAGAGGAGAAGCTCAAGCTGG-3′; T91A reverse, 5′-CCTCTGGGGCGGCCTTGAAGAAGGGCTCACT-3′; *T466A* forward, 5′-TATTTTCGCCCCACTGCTGCACCAGATT GAG-3′; *T91A* reverse, 5′- GCAGTGGGGCGAAAATACGCCAGG CCTCAC-3′. *T91D* forward, 5′-CAAGGCCGACCCAGAGGA GAAGCTCAAGCTGG-3′, *T91D* reverse, 5′-CCTCTGGGTCGGC CTTGAAGAAGGGCTCACT-3′; *T91E* forward, 5′-CAAGGCC-GAACCAGAGGAGAAGCTCAAGCTGG-3′, *T91E* reverse, 5′-CC TCTGGTTCGGCCTTGAAGAAGGGCTCACT-3′; *D144N* forward, 5′-GGAGCTGAAATTGGCTAATTTTGGCCTGGCTCG -3′; *D144N* reverse, 5′-CGAGCCAGGCCAAAATTAGCCAATT TCAGCTCC-3′. All transfection experiments were conducted with Lipofectamine 2000 (Thermo Fisher Scientific, cat. no. L3000015) as recommended by the manufacturer. MDA-MB-231 cells were transfected with lentiviruses containing *CDK5*, *G6PD-WT*, *G6PD-T91A*, *G6PD-T91D*, *G6PD-T91E* and *G6PD-T466A* vectors, and stable cell lines were obtained after treatment with 2 mg/mL puromycin for 7 days.

2.5. CRISPR-CAS9 knockout

Online sgRNA Designer were used (http://chopchop.cbu.uib.no/). To target the common exons for all human *CDK5* isoforms were synthesized as follows: 5′-GGCCTTGAACACAGTTCCGT-3′; To target the common exons for all human *G6PD* isoforms were synthesized as follows: 5′-GTGTGTATCCGACTGATGGA-3′. All SgRNAs were cloned to lentiCRISPRv2 (one vector system) plasmids from Zhang lab. Scramble sequence: 5′-GCGTGA-CAGCTCGCTTCATA-3′.

2.6. Protein extraction, immunoblotting, and antibodies

Protein was extracted with cell lysis buffer for Western blotting and IP (Beyotime, cat. no. P0013). Briefly, scraped cells were collected after centrifugation at 1000×*g* for 3 min. The pelleted cells were lysed in cell lysis buffer containing proteinase and phosphatase inhibitors (MCE, cat. no. HY-K0010, cat. no. HY-K0021, respectively) for 15 min on ice. The supernatant was transferred to a new tube, and the protein concentration was measured using a BCA Protein Assay Kit (Beyotime, cat. no. P0012S). SDS-PAGE and immunoblotting were performed as described previously[53]. The following antibodies were used: G6PD (Proteintech, 25413-1-AP); PARP (Cell Signaling Technology, cat. no. #9532); active caspase-3 (Cell Signaling Technology, cat. no. #9662); CDK1 (Proteintech, cat. no. 19532-1-AP); CDK2 (Proteintech, cat. no. 22060-1-AP); CDK5R1 (Proteintech, cat. no. 67503-1-lg); CDK5 (Proteintech, cat. no. 10430-1-AP); γH2AX (Proteintech, cat. no. 10856-1-AP); HA tag (Proteintech, cat. no. 66006-2-lg); Flag tag (Proteintech, cat. no. 66008-3-lg); phospho-threonine-proline mouse mAb (Cell Signaling Technology, cat. no. #9391), 6PGD (Proteintech, cat. no. 14718-1-AP), PGLS (Proteintech, cat. no. 30560-1-AP), β-actin (Kangchen, cat. no. KC-5A08), and GAPDH (Kangchen, cat. no. KC-5G4).

2.7. In vitro kinase assay

Human CDK5/p35 complex was purchased from Promega (cat. no. V3271), and human G6PD recombinant protein was purchased from Genetex (cat. no. GTX66999-pro). An *in vitro* kinase assay was performed as described before[28]. Briefly, the *in vitro* kinase assay was conducted in a 1 × kinase buffer (Cell Signaling Technology, cat. no. 9820S) supplemented with 1 μmol/L $CaCl_2$ and 10 μmol/L ATP (Cell Signaling Technology, cat. no. 9804S). In each reaction tube, 50 ng G6PD was incubated with 10 or 50 ng CDK5/P35 proteins with or without adding GFB-12811 (10 μmol/L) or G6PDi-1 (10 μmol/L) as indicated at 30 °C for 2 h. The tube maintained on ice was used as a negative control. Histone H1 (Abcam, cat. no. ab198676) was loaded as a positive control. The reaction products were subjected to Western blotting for further identification.

2.8. Phosphorylated peptides identification

The phosphorylated peptide identification was performed as described before[28]. Briefly, the phosphorylated G6PD derived from the *in vitro* kinase assay was digested by Lys-C (1:100, *w*/*w*) at 37 °C for 3 h followed by trypsin (1:50, *w*/*w*) overnight at 37 °C. The resulting peptides were dissolved in 0.2% formic acid (FA) separated using an online Nano-LC system (Microtech Scientific) and equipped with a C18 reversed-phase column. Then, they were subjected to an LTQ-Orbitrap mass spectrometer (ThermoFisher). Full-scan spectra were acquired at a target value of 4×10^5 with a resolution of 60,000. Data were acquired in a data-dependent acquisition mode using the top-speed method (3 s). The peptides were isolated using a quadrupole system (the isolation window was 0.7). Raw files were analyzed *via* MaxQuant software. Peak lists were searched against the UniProt protein sequence database.

2.9. G6PD monomer and dimer detection

DSS crosslinking assay was used to detect the G6PD dimer as described before[54]. Briefly, His-tag fused WT G6PD or T91A mutated G6PD expression vectors were transfected into MDA-MB-231 cells and were cultured under glucose deprivation to induce CDK5-mediated phosphorylation of G6PD. Cells were trypsinized and washed twice by cold PBS. Then, cells were suspended in conjugation buffer (20 μmol/L HEPES, pH = 8.0) with DSS (a final concentration of 1 μmol/L). After incubation at 37 °C for 30 min, the total protein was extracted from the cells and subjected to Western blotting for detection of G6PD monomer and dimer.

2.10. Preparation of the polyclonal antibody against pho-G6PD at Thr-91

A phosphorylated peptide fragment of G6PD (SEPFFKA(pTHR) PEEKLKLEDFFC) was synthesized and fused with KLH by GenScript. The purified fusion peptide was used to immunize female BALB/c mice according to the conventional procedure. The serum containing anti-pho-G6PD at Thr-91 was purified using Protein G affinity chromatography. Specificity and titration of the antibody were assessed by Western blotting and IHC in cells and tissues with different levels of pho-G6PD.

2.11. RNA extraction and qPCR analysis

Total RNA was isolated from cells or tissues by TRIzol Reagent (Invitrogen, cat. no. 15596018), and 1 mg of RNA from each sample was reverse transcribed to generate cDNA using a Prime Script RT Master Mix Kit (Takara, cat. no. RR036Q). Next, 1 mL (50 ng) cDNA was used as a template for qPCR with AceQ Universal SYBR qPCR Master Mix (Vazyme, cat. no. Q511-02) according to the manufacturer's instructions. The primers used in our study are listed in the Supporting Information Table S1.

2.12. Tissue microarray and immunohistochemical staining

Tissue microarray sections (Human breast cancer tissue microarray, HBreD090CS01) were purchased from Shanghai Outdo Biotech Co., Ltd. (National Human Genetic Resources Sharing Service Platform, 2005DKA21300). This study was approved by the Institutional Review Board at Nanjing University. Tissue sections were immunostained with the antibody generated in this study for the detection of CDK5 expression and G6PD phosphorylation.

Immunohistochemistry experiments were performed as previously described[55]. Formalin-fixed, paraffin-embedded tumor tissue sections were prepared according to the manufacturer's instructions. Antigens were retrieved by boiling the slides in 0.01 mol/L sodium citrate (pH 6.0) in a microwave for 15 min, after which the tissue sections were washed three times in 1 × PBS/0.1% Tween-20 (PBST) solution. Consecutively, the slides were incubated for 1 h at room temperature in blocking solution (5% BSA in 1 × PBST), followed by overnight incubation at 4 °C in blocking solution in which primary antibodies were diluted (1:400). The sections were then washed three times using 1 × PBST solution and incubated at room temperature for 1−2 h in blocking solution in which HRP conjugated secondary antibodies were diluted.

A semiquantitative Histoscore was calculated for each specimen by multiplying the distribution area (0−100%) at each staining intensity level by the intensity (0, negative; 1, weak staining; 2, moderate staining; and 3, strong staining) as previously reported[56].

2.13. Cell proliferation, viability assay, and apoptosis analysis

To detect cell proliferation, 5×10^3 transgenic MDA-MB-231 cells (overexpressing CDK5, G6PD-WT, and G6PD-T91A) were seeded in a volume of 100 mL medium per well on a 96-well plate. After culturing for the indicated period, cell proliferation was measured using a Cell Counting Kit 8 (CCK-8; Beyotime, cat. no. C0037) according to the manufacturer's instructions. For the measurements of cell viability under treatment with H_2O_2 or anticancer agents, cells were seeded in 96-well plates (2×10^4 cells/well) in the presence or absence of the indicated treatments. Cell viability was evaluated using the CCK-8 kit mentioned above. The optical density (OD) value was read at 450 nm. Fold changes were calculated using the baseline values of untreated cells as a reference (set to 100%). For the measurement of apoptosis induced by H_2O_2 and other treatments, 2×10^6 MDA-MB-231 cells were seeded in 6-well plates and cultured under normal conditions or in glucose deprivation medium. After treatment with H_2O_2 or anticancer agents, the cells were harvested and stained with an Annexin V-FITC/PI Apoptosis Detection Kit (Vazyme, cat. no. A211-01), followed by flow cytometry measurement of fluorescence.

2.14. TUNEL analysis

Apoptosis was detected in tumor tissues by TUNEL assay. Tissue sections were incubated with TdT/dUTP at 37 °C for 30 min, washed, and incubated at room temperature with HRP-conjugated anti-Digoxigenin for 30 min. Representative images from each stained section were captured using an Olympus BX43 microscope.

2.15. G6PD and 6PGD activity measurement

G6PD activity was assayed using the G6PD Activity Assay Kit with WST-8 (Beyotime, cat. no. S0189) according to the manufacturer's instructions. Briefly, cells were harvested and lysed after indicated treatments using G6PD Extracting Solution (Beyotime, cat. no. S0189-5). The lysates were centrifuged (12,000×g, 15 min, 4 °C) and subjected to BCA assay for measuring protein concentration. The G6PD activity was measured from the obtained supernatants in the reaction mix containing (final concentration) 50 μmol/L KPi (potassium phosphate buffer, pH = 7.5), 0.5 μmol/L EDTA, 5 μmol/L $MgCl_2$, 2 μmol/L G6P, 0.2 μmol/L $NADP^+$ and 10 mg of sample protein. The formed NADPH rapidly reduced WST-8 to produce a formazan product, which could be determined by monitoring absorbance in the 430−550 nm range. The G6PD activity was calculated according to the standard curve and normalized to protein concentration.

6PGD activity was evaluated by using 6PGD Activity Colorimetric Assay Kit (Solarbio, cat. no. BC2100, China). In this assay, the conversion of 6-phosphogluconate from 6PGD generated NADPH, which subsequently reduced a colorless probe to a colored product detectable by absorbance at 450 nm.

2.16. GSH/GSSG ratio measurements and intracellular ROS, NADPH, and $NADP^+$ production

The total intracellular ROS level was determined as described previously[25]. Briefly, cells were incubated with 10 μmol/L 2′,7′-dichlorodihydrofluorescein diacetate (H_2-DCFH-DA, Thermo Fisher Scientific, cat. no. D399) at 37 °C for 30 min. Next, the cells were harvested, washed twice with ice-cold PBS, resuspended in PBS, and subjected to flow cytometry. Intracellular NADPH and $NADP^+$ levels were determined using a $NADP^+$/NADPH Assay Kit with WST-8 (Beyotime, cat. no. S0179), and the GSH/GSSG ratio was determined using a GSH/GSSG Assay Kit (Beyotime, cat. no. S0053).

2.17. Anoikis and soft agar colony formation assay

Anoikis was induced by plating cells (10^6 cells/well) on ultralow attachment 6-well plates (Corning, cat. no. 3471). For the soft agar colony formation assay, the cell suspension was mixed with 0.7% soft agar in 2 × DMEM containing 20% FBS in an equal volume and layered in triplicate onto 1.4% solidified agar in 2 × DMEM containing 20% FBS. After 14 days of cell culture, the colonies were counted under a microscope and photographed.

2.18. In vivo tumorigenesis and metastasis assays

For the *in vivo* tumorigenesis experiments, all female nude mice (6−7 weeks old) were purchased from the Model Animal Research Center of Nanjing University (Nanjing, China). 1×10^7 cells in 200 mL PBS with 30% Matrigel (BD, 356234) were subcutaneously injected into mice, and mice were randomly allocated to the groups. When tumor volume reached ∼100 mm^3, mice were treated with indicated treatments. Tumor volumes and body weights were recorded. The animal care and experimental procedures of the animal studies were approved by the Laboratory Animal Welfare and Ethics Committee of Nanjing University and carried out at Nanjing University (Accreditation No. IACUC-2007015). All animal experiments conformed to the guidelines of the Animal Care and Use Committee of Nanjing University. All efforts to minimize suffering were made. Subcutaneous administration was performed as reported previously[25].

Cells were stably transfected with the firefly luciferase gene for the lung metastasis model. 5×10^6 cells were resuspended in 200 mL of sterile PBS and subsequently injected into the tail veins of nude mice. Lung colonization was monitored at the indicated time point after intraperitoneal injection of D-luciferin (MCE, cat. no. HY-12591A) with a Lumina XR IVIS bioluminescent imaging system. After 28 days, mice were sacrificed *via* cervical dislocation, and the lungs were collected and paraffin-embedded to allow histopathological examination of metastatic nodules.

2.19. Statistical analysis

All statistical analyses were performed by GraphPad Prism 5 (GraphPad). Differences between the two groups were assessed by Student's *t*-test. Multiple comparisons between two populations were conducted by multiple *t*-test with type 1 error correction. Differences among multiple groups were assessed by one- or two-way ANOVA. Differences between tumor growth curves were determined by repeated measures of two-way ANOVA. The significance threshold was $P < 0.05$. For all figures, $^*P < 0.05$, $^{**}P < 0.01$, $^{***}P < 0.001$. All data are shown as mean ± standard deviation (SD) unless noted in the figure legend. Generally, all *in vitro* experiments were carried out with $n \geq 3$ biological replicates.

3. Results

3.1. CDK5 induces augmentation of PPP flux in BC cells

Our previous GSEA analysis (GEO Accession number GSE132902)[16] indicated that CDK5 potentially promoted PPP in BC cells (Supporting Information Fig. S1A). To decipher the role of CDK5 in glucose metabolism, we analyzed whether CDK5 affected glucose consumption and lactate production in BC cell line MDA-MB-231. To this end, we treated MDA-MB-231 cells with either CDK5 inhibitor Roscovitine (Rosc) a commercial CDK5 inhibitor, or GFB-12811 a selective CDK5 inhibitor[17]. These treatments were used to suppress CDK5 activity in the cells. In MDA-MB-231 cells, our results showed that CDK5 inhibition significantly increased lactate production compared to that of the DMSO group (Fig. 1A, right). In contrast to CDK5 overexpression (Fig. S1B), which substantially decreased lactate secretion (Fig. 1B, right), both treatments had little effect on glucose uptake (Fig. 1A and B). Interestingly, overexpression of CDK1 or CDK2, the two other potential targets of Rosc, had no significant effects on glucose uptake and lactate secretion in MDA-MB-231 cells (Fig. S1C and S1D). Furthermore, CDK5 knockout *via* CRISPR/CAS9 gene editing in MDA-MB-231 cells (Fig. S1B) induced the same regulation of glucose metabolism as compared with CDK5 inhibitors (Fig. S1E). Similar results were observed in another BC cell line, MCF-7 (Fig. S1F). These results indicated that CDK5 had functional significance in regulating glucose metabolism in BC cells. To better understand how CDK5 affected glucose metabolism, we identified critical factors involved in glucose metabolism that could be potentially regulated by CDK5. As shown in Fig. S1G, CDK5 inhibition conspicuously affected the expression levels of multiple enzymes, TP53-induced glycolysis regulatory phosphatase (*TIGAR*) was the most affected. It is plausible that compensatory *TIGAR* expression aims to protect tumor cells by reducing glycolytic rates and diverting glycolytic intermediates into the PPP[18], which was suppressed by CDK5 inhibition. Moreover, increased glucose flux through the oxidative PPP has been shown to decrease lactate excretion[19]. Thus, we speculated that CDK5 would bias glucose metabolic flux towards the PPP.

To determine whether CDK5 activation shifted BC cell glucose metabolism to the PPP, we performed isotopomer spectral analysis (ISA) in MDA-MB-231 cells using liquid chromatography/mass spectrometry (LC/MS) to trace ^{13}C labels from 1,2-$^{13}C_2$ glucose (Fig. 1C), as previously described[20]. The major intermediate metabolites of glycolysis and PPP were subsequently analyzed to determine the fate of glucose carbon (Fig. 1D). In the PPP, the C1 carbon of incoming glucose is released as CO_2 during the conversion of 6-phosphogluconate to ribulose-5-phosphate (Ru5P), indicating that metabolites in the PPP carry one ^{13}C-labelled carbon. In contrast, glycolytic intermediates and products carry two labels (Fig. 1C)[21]. According to our accurate quantification of isotopologue distribution in BC cells with CDK5 overexpression, we found that ^{13}C-enrichment of the G6P [M+2] isotopologue was markedly downregulated in comparison with that of the control group. In contrast, the fructose-6-phosphate (F6P) [M+2] isotopologue and fructose-1,6-bisphosphate (FBP) [M+2] isotopologue showed minimal changes (Fig. 1E and F, Fig. S1H). However, we observed no significant alterations in the ^{13}C-enrichment of the G6P [M+2] isotopologue in BC cells with CDK5 inhibition *via* either Rosc or GFB-12811 (Fig. 1E). This could be attributed to the low expression level of CDK5 in BC cells under normal conditions (Fig. S1B). Considering that G6P is metabolized by both glycolysis and PPP, we inferred that the observed reduction in the G6P [M+2] isotopologue indicated possible utilization by the PPP. As expected, CDK5 overexpression strongly promoted the enrichment of Ru5P [M+1] isotopologue derived from 1,2-$^{13}C_2$ glucose (Fig. 1G), which is the end product of the oxidative branch of the PPP[5]. In contrast, inhibition of CDK5 reduced the abundance of the Ru5P [M+1] isotopologue in comparison with that of the control group

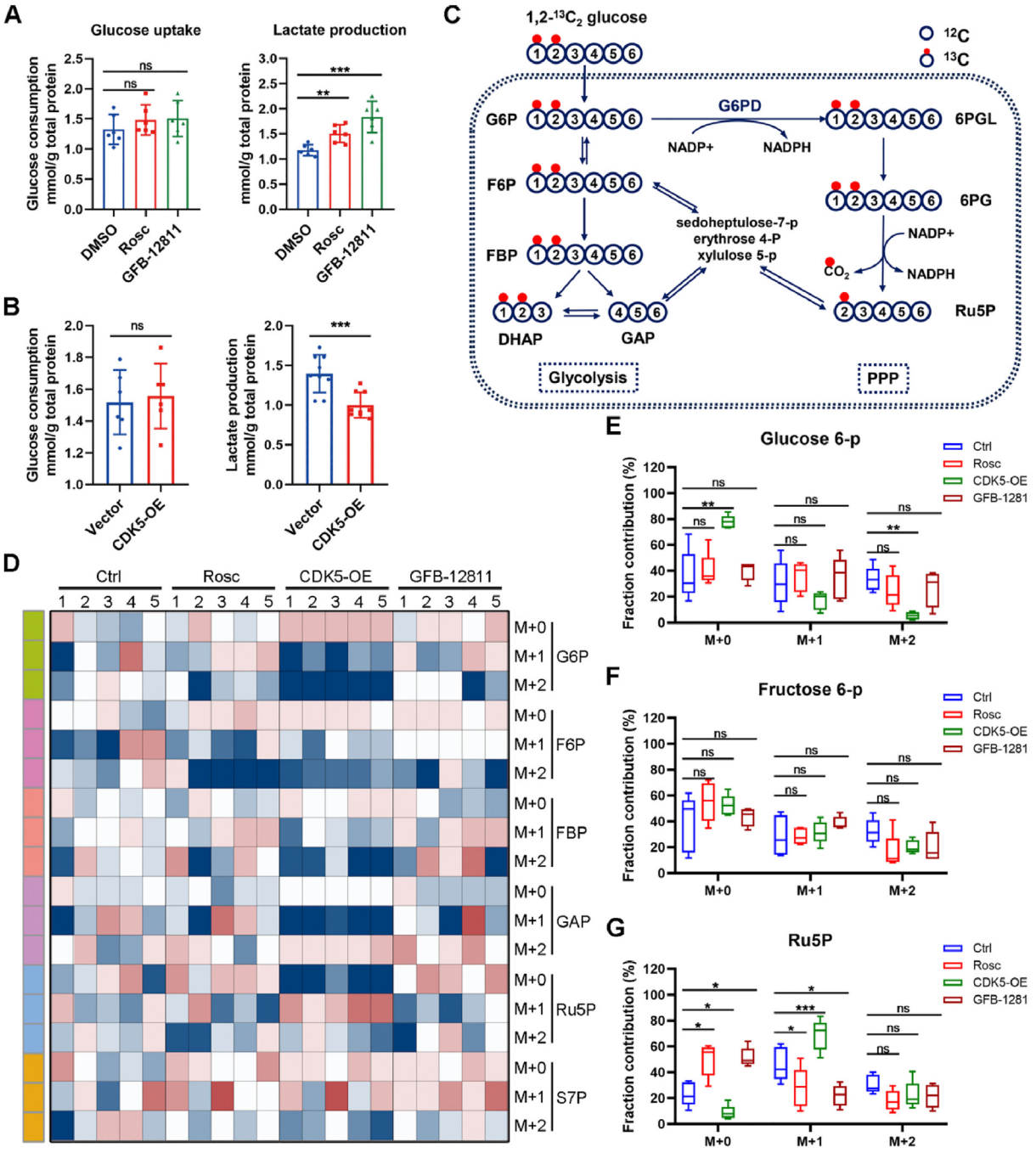

Figure 1 CDK5 induces augmentation of PPP flux in BC cells. (A, B) Glucose consumption and lactate production of MDA-MB-231 cells after incubation with CDK5 inhibitor, Roscovitine (10 mg/mL), and GFB-12811 (10 mg/mL) ($n = 6$) for 24 h (A). MDA-MB-231 cells were transfected with a CDK5-expression vector. Glucose consumption and lactate production were analyzed ($n = 6$) (B). Total protein was used for normalization. DMSO treatment and transfection of the backbone vector were used as controls. (C−G) Isotopomer spectral analysis in MDA-MB-231 cells by using LC/MS to trace ^{13}C labels from 1,2-$^{13}C_2$ glucose. Schematic image of atom mapping for 1,2-$^{13}C_2$ glucose tracing glycolysis, oxidative PPP, and non-oxidative PPP (C). White balls are ^{12}C atoms. Shaded balls are ^{13}C atoms, in which ^{13}C atoms first entering oxidative PPP are red, and those first entering glycolysis are blue. Heatmap of metabolite levels from MDA-MB-231 cells with the indicated treatments (Ctrl, transfected by vector and treated with DMSO; Rosc, transfected by vector and treated with 10 mg/mL Rosc; CDK5-OE, overexpressed CDK5 and treated with DMSO; GFB-12811, transfected by vector and treated with 10 mg/mL GFB-12811) (D). Boxplots of the fractional contributions of G6P (E), F6P (F), and Ru5P (G) within the [M+0], [M+1] and [M+2] isotopologues derived from 1,2-$^{13}C_2$ glucose extracted from MDA-MB-231 cells with indicated treatment, ($n = 5$). Data are presented as mean ± SEM. Statistical significance was calculated using the one-way ANOVA (A), the student's *t*-test (B), and the two-way ANOVA (E−G). ns, not significant, $^*P < 0.05$; $^{**}P < 0.01$; $^{***}P < 0.001$.

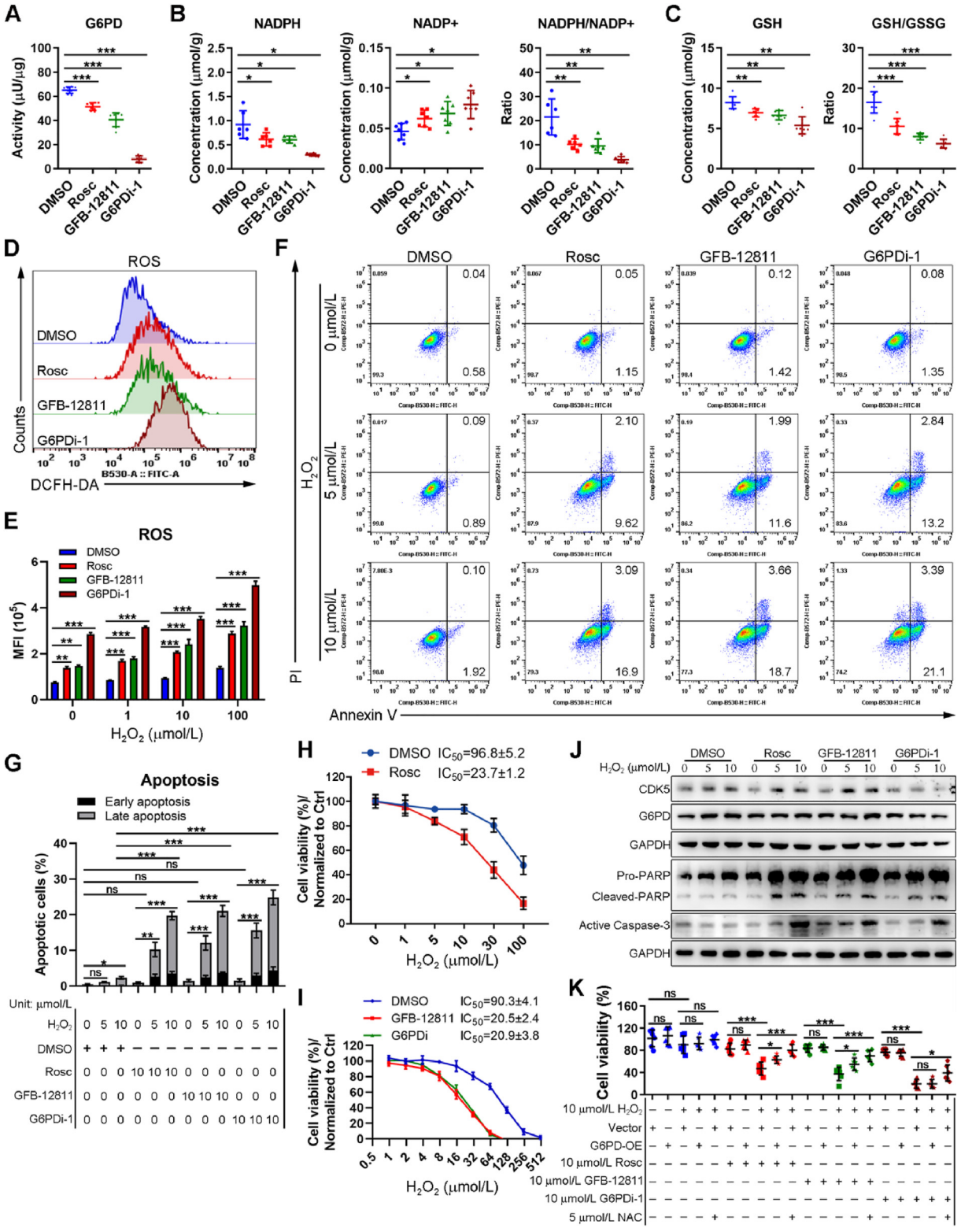

Figure 2 CDK5 consolidates intracellular redox homeostasis by enhancing G6PD activity. (A−C) MDA-MB-231 cells were treated with Rosc (10 μmol/L), GFB-12811 (10 μmol/L), and G6PDi-1 (10 μmol/L) for 24 h G6PD enzymatic activity (A), intracellular NADPH and NADP + production, the NADPH/NADP + ratio (B), the GSH level, and the GSH/GSSG ratio ($n = 6-8$) (C) were examined *via* indicated kits. Total protein was used for normalization. (D−E) Flow cytometric analysis of ROS level in cells from (A). A representative image is shown (D). Intracellular ROS levels in tumor cells incubated with indicated treatment, plus different concentrations of H_2O_2, were tested *via* flow cytometry and semi-quantified according to MFI (E) ($n = 4$). (F, G) Apoptosis in cells from (E) was analyzed *via* flow cytometry ($n = 3$). Representative images (F) and quantification data (G) are shown. (H, I) H_2O_2 dose-response curve of tumor cells exposed to the indicated treatment.

(Fig. 1G). These results show that CDK5 enhanced the activity of the PPP oxidative branch, which competitively metabolized G6P and subsequently produced Ru5P.

3.2. CDK5 consolidates intracellular redox homeostasis by enhancing G6PD activity

To explore how CDK5 promoted the activity of the PPP, the expression and catalytic activity levels of three rate-limiting enzymes in the PPP were examined, including G6PD, 6-phosphogluconate dehydrogenase (6PGD), and 6-phosphogluconolactonase (PGLS)[3]. Of note, CDK5 inhibition did not affect the expression of these genes in MDA-MB-231 cells (Supporting Information Fig. S2A and S2B). In contrast, it significantly reduced G6PD catalytic activity (Fig. 2A), without affecting 6PGD (Fig. S2C). To serve as a positive control, a G6PD-selective inhibitor, G6PDi-1, was employed (Fig. 2A). To further substantiate the role of CDK5 in G6PD activation, we aimed to determine whether CDK5 interruption disrupted redox balance. To accomplish this, redox status was assessed by measuring the antioxidant capacity of tumor cells. As shown in Fig. 2B, the presence of CDK5 inhibitors led to a significant decrease in NADPH levels and a corresponding increase in $NADP^+$ levels. Similar results were observed in the G6PDi-1-treated group (Fig. 2A and B). Insufficient NADPH production limited the regeneration of GSH from its oxidized form, GSSG (Fig. 2C, Fig. S2D). Moreover, consistent with the trends shown by NADPH and GSH, the intracellular ROS level was elevated after CDK5 inhibition or G6PD inhibition (Fig. 2D). These results indicate that CDK5 inhibition was of great potential to break the redox balance in BC cells, potentially by modulating G6PD activity.

To our knowledge, dysregulation of redox balance induces intracellular ROS accumulation, which is harmful to rapidly proliferative cancer cells[22]. Thus, cancer cells adaptively execute several alternative pathways to overcome oxidative stress, such as *mTOR*, *NRF2*, and *p53*[23]. In neurodegenerative diseases, CDK5 was previously found to be hyperactivated under oxidative stress[24], indicating that CDK5 might be a potential regulator in intracellular redox homeostasis. Indeed, in this study, we observed that CDK5 inhibition significantly enhanced intracellular ROS production (Fig. 2E) and promoted the susceptibility of BC cells to H_2O_2 treatment, resulting in remarkable apoptosis (Fig. 2F–I). In support of this finding, Western blotting revealed that exposure to H_2O_2 caused typical PARP1 proteolytic cleavage and elevated the expression of activated caspase-3 in BC cells after CDK5 inhibition compared to the control group (Fig. 2J). Moreover, 10 μmol/L H_2O_2, a nonlethal dose for MDA-MB-231 cells, significantly suppressed cell viability when combined with CDK5 inhibition or G6PD suppression (Fig. 2H and I). The forced expression of G6PD (Fig. S2E) or administration of the antioxidant *N*-acetyl-L-cysteine (NAC) significantly decreased intracellular ROS levels (Fig. S2F), maintained redox balance (Fig. S2G) and completely restored cell viability (Fig. 2K, Fig. S2H and S2I). More importantly, we noticed that after H_2O_2 administration in MDA-MB-231 cells, CDK5 expression was elevated in an H_2O_2 dose-dependent manner (Fig. 2J). In contrast, the G6PD protein level remained unchanged, which strengthened the hypothesis that CDK5 might be a potential regulator in intracellular redox homeostasis. Indeed, CDK5 knockout attenuated the increase in G6PD activity, as well as NADPH production in MDA-MB-231 cells with incubation of 10 μmol/L H_2O_2 (Fig. S2J and S2K), resulting in high ROS production (Fig. S2L). Similar results were also observed in MCF-7 cells (Supporting Information Fig. S3A). Collectively, these data illustrate that CDK5 promoted G6PD activation and was crucial for the maintenance of intracellular redox homeostasis in BC cells.

3.3. CDK5 protects BC cells against glucose deprivation

Like H_2O_2 treatment, glucose deficiency elicits oxidative stress and induces apoptosis of tumor cells[25]. As described above, the link between CDK5 and redox homeostasis suggested that BC cells could be vulnerable to CDK5 inhibition under glucose deprivation. To test this hypothesis, we developed and established a cellular model of glucose deficiency by culturing cancer cells on a glucose-deficient medium. Consistent with a previous report[26], glucose deprivation significantly elevated the intracellular ROS level of MDA-MB-231 cells and induced potent apoptosis (Fig. 3A–D). Then, we examined the effect of CDK5 inhibition during glucose deprivation by treating MDA-MB-231 cells with Rosc and GFB-12811, respectively. As shown in Fig. 3E, G6PD activity significantly increased in MDA-MB-231 cells under glucose deprivation compared with that in a standard medium. In contrast, CDK5 inhibition greatly attenuated the increase of G6PD activity induced by glucose deprivation (Fig. 3E), which promoted ROS enrichment (Fig. 3D) and facilitated apoptosis (Fig. 3B and C). Correspondingly, NADPH and reduced GSH production were also significantly decreased after interruption of CDK5 activity, which was also observed in G6PDi-1-treated cells (Fig. 3F and G, Fig. S3B and S3C).

To further validate the findings described above, we evaluated the sensitivity of MDA-MB-231 cells to glucose deprivation by using a conditioned medium with varying concentrations of glucose. MDA-MB-231 cells were cultured in the conditioned medium as indicated (Fig. 3H). As shown in Fig. 3H, complete glucose deprivation did not alter MDA-MB-231 cell survival within 6 h. However, CDK5 inhibition (red line and green line) induced cell death when the concentration of glucose was 200 mg/L or lower (Fig. 3H). Notably, the reduction in cell viability following Rosc or GFB-12811 treatment under glucose deprivation was remarkably ameliorated by G6PD overexpression (Fig. 3H). Interestingly, during glucose deprivation, intracellular CDK5 expression (Fig. 3I) and G6PD activity (Fig. 3E) were simultaneously elevated. Moreover, CDK5 inhibition or G6PD

MDA-MB-231 cells (10^5 cells/well) were pretreated with CDK5 inhibitor (Rosc, 10 μmol/L; GFB-12811, 10 μmol/L; G6PDi-1, 10 μmol/L) for 12 h, and subsequently added with indicated concentration of H_2O_2 for 24 h. Cell viability was determined *via* CCK-8 assay. The IC_{50} was calculated. (J) Immunoblot analysis of apoptosis-related protein, pro-/cleaved-PARP, and active caspase-3 expression in BC cells exposed to the indicated treatment described in (H, I). β-Actin was used as a loading control. (K) MDA-MB-231 cells (10^5 cells/well) were transfected with G6PD-expression vector and subsequently incubated with Rosc (10 μmol/L), GFB-12811 (10 μmol/L), G6PDi-1 (10 μmol/L), plus 10 μmol/L H_2O_2 for 24 h, with or without NAC (5 μmol/L). Cell viability was examined *via* CCK-8. Data are presented as mean ± SEM. Statistical significance was calculated using the One-way ANOVA (A–C, G, and K) and the two-way ANOVA (E, H, I). ns, not significant, $^*P < 0.05$; $^{**}P < 0.01$; $^{***}P < 0.001$.

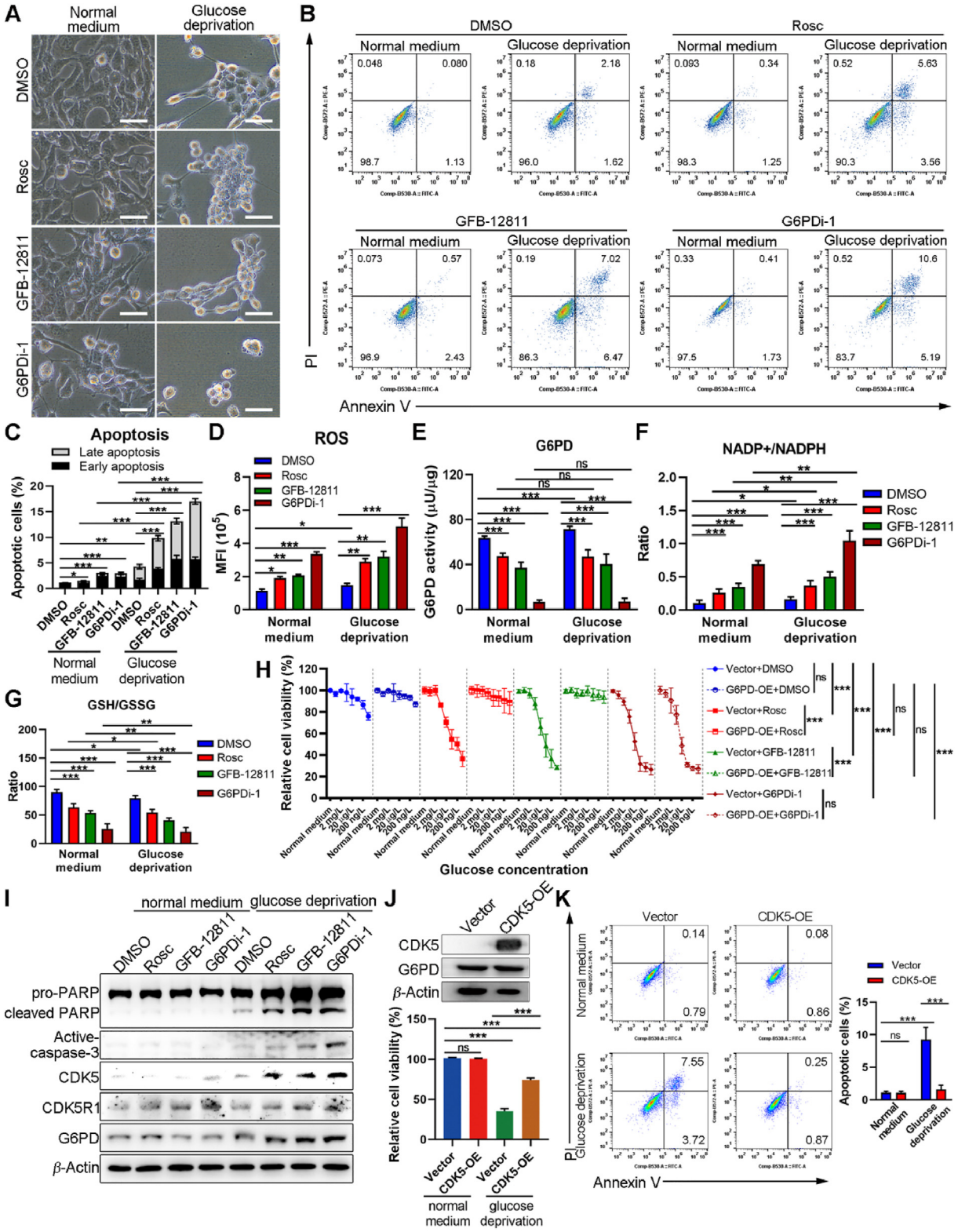

Figure 3 CDK5 protects BC cells against glucose deprivation. (A) Bright-field images of MDA-MB-231 cells cultured in glucose deprivation medium containing Rosc (10 μmol/L), GFB-12811 (10 μmol/L), or G6PDi-1 (10 μmol/L) for 24 h. Scale bar = 20 μm. (B, C) Cells from (A) were subjected to flow cytometric analysis. Representative flow cytometric images (B) and quantification data (C) are shown (n = 3). (D–G) Intracellular ROS levels (D), G6PD activity (E), ratio of $NADP^+$/NADPH (E), and ratio of GSH/GSSG (G) in cells from (A) were examined (n = 6). (H) MDA-MB-231 cells were transfected with G6PD or the vector control and then pretreated with Rosc (10 μmol/L), GFB-12811 (10 μmol/L), or G6PDi-1 (10 μmol/L) for 24 h, subsequently cultured with the glucose-free medium. Different concentrations of glucose were supplemented. Cell viability was examined *via* CCK-8 assay. (I) Immunoblot analysis of apoptotic marker (pro/cleaved-PARP, active

suppression significantly sensitized BC cells to oxidative stress induced by glucose deprivation. Furthermore, transient expression of CDK5 also protected MDA-MB-231 cells against glucose deprivation-induced apoptosis (Fig. 3J and K). Similar results were observed in MCF-7 cells (Fig. S3D−S3F). Collectively, these findings illustrate that CDK5-induced G6PD activation influenced redox homeostasis and enabled BC cells to survive during glucose deprivation.

3.4. CDK5-induced phosphorylation of G6PD at Thr-91 facilitates G6PD activation and promotes tolerance to oxidative stress

Next, we endeavored to identify the mechanism by which CDK5 facilitated G6PD activation. As mentioned above, G6PD expression remained unchanged at both the transcriptional and translational levels after CDK5 interruption (Fig. S2A−S2D, Fig. 2J). Thus, we hypothesized that CDK5 might induce post-translational modification (PTM) of G6PD, which could be able to modulate its catalytic activity[27]. As expected, the phosphorylation level of G6PD was tightly influenced by CDK5 (Fig. 4A). These data illustrated the essential role of CDK5 in regulating G6PD phosphorylation. To provide further validation, we performed an *in vitro* kinase assay as previously reported[28]. As shown in Fig. 4B, G6PD phosphorylation was elevated in the presence of CDK5/P35 complex, notably abrogated by the administration of CDK5 inhibitors or G6PD inhibitors. Moreover, silencing CDK5 kinase activity *via* D144N mutation (a catalytically inactive mutant)[29] failed to mediate G6PD phosphorylation (Supporting Information Fig. S4). Next, we determined to validate the amino acid residue that was potentially phosphorylated by CDK5. To our knowledge, CDK5 is known to be a proline-directed protein kinase that mediates phosphorylation on serine or threonine residues in substrates, specifically within the consensus motif S/TPXH/K/R[13]. By using a group-based prediction system[30], a comprehensive tool for predicting phosphorylation sites, two threonine residues followed by proline, Thr-91, and Thr-466, were identified as potential phosphorylation targets (Fig. 4C). For further exploration, threonine residues Thr-91 and Thr-466 were mutated to Ala to generate the T91A and T466A mutations, respectively, transfected them into MDA-MB-231 cells. The exogenous wild-type G6PD protein or mutated G6PD protein was isolated *via* co-immunoprecipitation and was furtherly analyzed by immunoblotting with P-Thr-Pro-101 mAb (CST, #9391), a mouse monoclonal antibody explicitly targeting phospho-threonine, not serine, only when followed by proline[31]. As a result, the T91A mutation completely abolished CDK5-mediated phosphorylation of G6PD. In contrast, the T466A mutation had little effect (Fig. 4D). For further validation, we performed an *in vitro* kinase assay coupled with HPLC−MS/MS analysis as described before[28]. As shown in Supporting Information Fig. S5, G6PD was exclusively phosphorylated at the T91 site. Although T466 has been reported to be phosphorylated by ASKa in Arabidopsis[32], it might have little contribution to CDK5-mediated G6PD phosphorylation in BC cells. Moreover, overexpression of CDK5 failed to enhance G6PD phosphorylation after T91A mutation (Fig. 4D). These results suggest that Thr-91 is crucial for CDK5-induced phosphorylation of G6PD. To further substantiate the findings described above, we generated a mouse polyclonal antibody against a recombinant peptide fragment of G6PD with phosphorylation at Thr-91 (98.8% protein identify, the peptide was synthesized by GenScript). The polyclonal antibody was evaluated through ELISA and immunoblotting (Fig. 4E, Supporting Information Fig. S6A and S6B). We observed that wide-type G6PD and mutated G6PD-T91E could be stained using the generated antibody, indicating that G6PD-T91E mutation exhibited the same conformation compared with phosphorylated G6PD-WT as described before[33]. By employing the generated polyclonal antibody, we found that phosphorylation of G6PD at Thr-91 was promoted after CDK5 overexpression and suppressed by Rosc treatment (Fig. 4E). These results show that Thr-91 is a potential target site for CDK5-mediated G6PD phosphorylation.

Next, we assessed the significance of the PTM described above in G6PD activation. To accomplish this, we generated MDA-MB-231 cells stably overexpressing either wildtype or mutated G6PD, as indicated in Fig. 4D. Transgenic cells were subsequently incubated under glucose deprivation. As expected, the enzymatic colorimetric assay showed that glucose deprivation significantly elevated G6PD activity (Fig. 4F). Conversely, genetic inhibition by T91A mutation dramatically decreased G6PD activity compared to that of WT G6PD. In contrast, the T466A mutation had little effect (Fig. 4F). More importantly, silencing G6PD phosphorylation by T91A mutation had a minimal impact on the basal activity of G6PD, compared with that of WT G6PD in a normal medium (Fig. 4F), suggesting that CDK5-mediated T91 phosphorylation played a partial modulatory role in G6PD activity. Furthermore, in agreement with the inhibitory effect of the T91A mutation on G6PD activity, NADPH and GSH production decreased by this mutation (Fig. 4G and H, Supporting Information Fig. S7A). As expected, antioxidant deficiency following the G6PD T91A mutation led to profound ROS elevation in the presence of oxidative stress (Fig. 4I, Fig. S7B and S7C), which resulted in mitochondrial damage (Fig. S7D) and subsequent apoptosis (Fig. 4J). In contrast, phosphorylation at Thr-91 significantly enhanced the tolerance of MDA-MB-231 cells to oxidative stress (Fig. S7C). Considering endogenous G6PD expression, which might interfere with the G6PD overexpression cell model, we genetically knockout endogenous G6PD in the MDA-MB-231 cells using CRISPR/Cas9 gene-editing tool (Fig. 4K). Subsequently, WT or mutated G6PD mimicking the persistent dephosphorylated (G6PD-T91A) or phosphorylated status (G6PD-T91D or G6PD-T91E)[34] were transfected into G6PD-KO cells (Fig. 4K), to establish transgenic MDA-MB-231 cell lines with G6PD T91 site-mutation. As expected, genetically, G6PD-T91A mutation significantly decreased G6PD activity compared with G6PD-WT and G6PD-T91E, rather than G6PD-T91D, which enhanced G6PD activity (Fig. 4K). More importantly, G6PD with T91A mutation still obtained activity at a basal level (Fig. 4K). These data validated a modulatory role of

caspase-3), CDK5, CDK5R1, and G6PD expression in cells from (A). β-Actin was used as a loading control. (J, K) MDA-MB-231 cells were transfected with CDK5 and the vector control and then were cultured with a normal medium or glucose-free medium for glucose deprivation for 24 h. Cells were harvested and subjected to immunoblot to analyze CDK5 and G6PD expression (J, top). Cell viability of the indicated cells cultured in glucose deprivation was determined by CCK-8 assay (H, bottom). Flow cytometry analyzed the apoptosis of cells from (J). Representative images and quantification data are shown (K). Data are presented as mean ± SEM. Statistical significance was calculated using the two-way ANOVA (C−H, J, K). ns, not significant, $^{*}P < 0.05$; $^{**}P < 0.01$; $^{***}P < 0.001$.

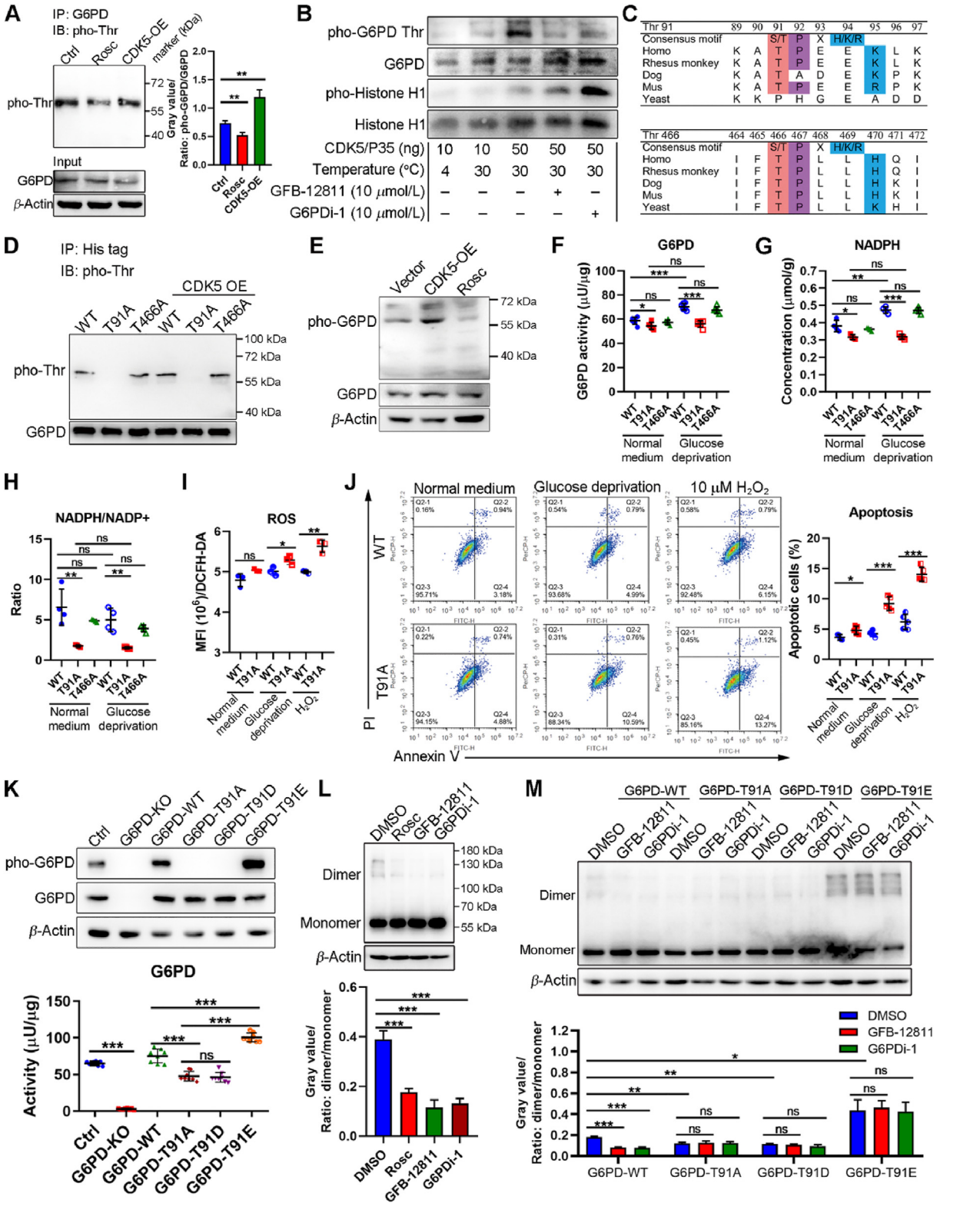

Figure 4 CDK5-induced phosphorylation of G6PD at Thr-91 facilitates G6PD activation and promotes tolerance to oxidative stress. (A) Immunoblot analysis of threonine phosphorylation of G6PD. MDA-MB-231 cells were transfected with CDK5-OE vector or incubated with Rosc (10 μmol/L) for 24 h. Total G6PD protein was immunoprecipitated and subsequently detected by P-Thr-Pro-101 mAb. Input G6PD was detected by anti-G6PD antibody. β-Actin was analyzed as a loading control. G6PD phosphorylation was semi-quantified (pho-G6PD/total G6PD) *via* ImageJ ($n = 3$). (B) *In vitro* kinase assay determined that CDK5 directly phosphorylated G6PD as described in the method. (C) G6PD threonine 91 and 466 are conserved and match with the CDK5 consensus motif. (D) MDA-MB-231 cells were transfected with His-tag-labelled G6PD-WT, G6PD-T91A, or G6PD-T466A, with or without CDK5 overexpression. The exogenous WT and mutated G6PD protein were purified *via*

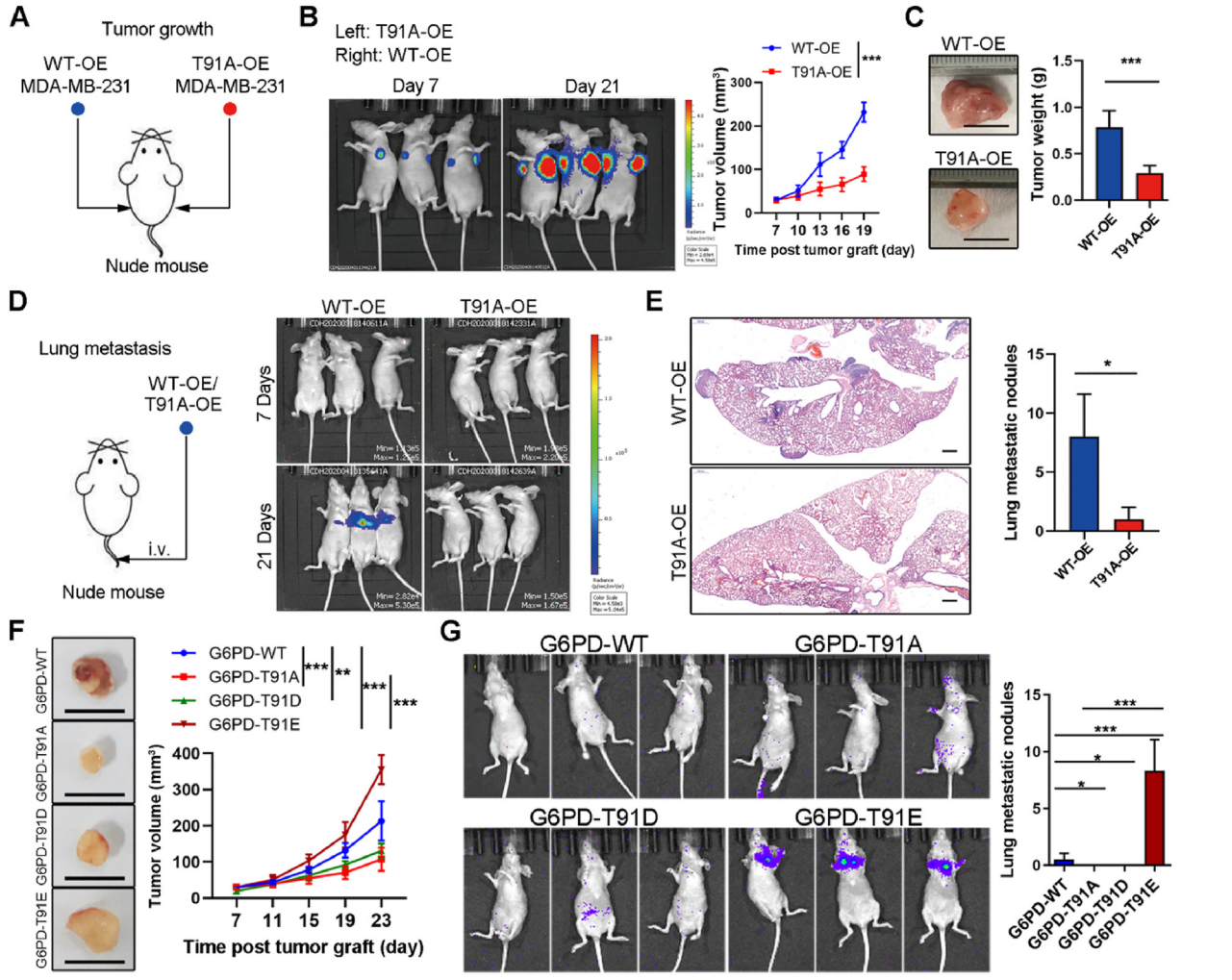

Figure 5 G6PD phosphorylation promotes tumor growth and lung metastasis of BC *in vivo*. (A) Schematic image of a xenograft mouse model established *via* implantation of MDA-MB-231 cells (5×10^6 cells/mouse) those overexpressing G6PD-WT (WT-OE), or G6PD-T91A (T91A-OE) respectively ($n = 6$). (B) Representative bioluminescence images of xenograft mice on Days 7 and 21 after tumor implantation (left). Mean tumor volume was recorded at the indicated times (right). (C) Representative photographs of tumor tissues isolated at the time of termination of the experiment (left; Scale bar = 1 cm). Tumor weight is presented (right). (D, E) WT-OE, T91A-OE cells from (A) were used for the establishment of a lung metastasis model *via* tail vein injection (2×10^6 cells/mouse) ($n = 6$). Metastatic progression was shown by bioluminescence imaging (D). Representative pictures of hematoxylin and eosin-stained (HE) sections of lung tissues (E, left). Quantification of pulmonary metastatic nodules (E, right). Scale bar = 500 μm. Data are presented as mean ± SEM. (F, G) Transgenic MDA-MB-231 cells with G6PD site mutation were used for the generation of a xenograft mouse model and lung metastasis model as described in (A) and (D) ($n = 6$). Representative photographs of tumor tissues isolated at the time of termination of the experiment (left; Scale bar = 1 cm) (F, left). Mean tumor volume was recorded at the indicated times (F, right). Representative bioluminescence images of xenograft mice on Days 7 and 21 after tumor implantation (G, left). Quantification of pulmonary metastatic nodules (G, right). Data are presented as mean ± SEM. Statistical significance was calculated using the student's *t*-test (C and E), one-way ANOVA (G), and two-way ANOVA (B, F). ns, not significant, $^*P < 0.05$; $^{**}P < 0.01$; $^{***}P < 0.001$.

BeyoGold His-tag Purification Resin and examined *via* immunoblotting as described in (A). Input G6PD was detected by an anti-G6PD antibody. (E) Immunoblotting analysis of G6PD phosphorylation at Thr-91 using mouse polyclonal antibody prepared in this study. G6PD was detected by an anti-G6PD antibody. β-Actin was used as a loading control. (F–J) MDA-MB-231 cells were transfected with G6PD-WT, G6PD-T91A, or G6PD-T466A and then were incubated using the normal medium and glucose-free medium, with or without H_2O_2 administration. G6PD (F), NADPH (G), ratio of NADPH/$NADP^+$ (H), ROS (I), and apoptosis (J) were determined. (K) Transgenic MDA-MB-231 cells with G6PD T91 site mutation were prepared for immunoblotting analysis of G6PD, pho-G6PD at the T91 site in prepared transgenic cells (top). G6PD activity in each cell line was examined (bottom) ($n = 6$). (L, M) MDA-MB-231 cells were pretreated as indicated and then incubated with 1 μmol/L disuccinimidyl suberate (DSS). The total protein was subsequently extracted and subjected to a Western blot to analyze dimeric and monomeric G6PD. The ratio (dimer/monomer) was calculated *via* ImageJ according to gray value. Data are presented as mean ± SEM. Statistical significance was calculated using the one-way ANOVA (A, K–M), and two-way ANOVA (F–J). ns, not significant, $^*P < 0.05$; $^{**}P < 0.01$; $^{***}P < 0.001$.

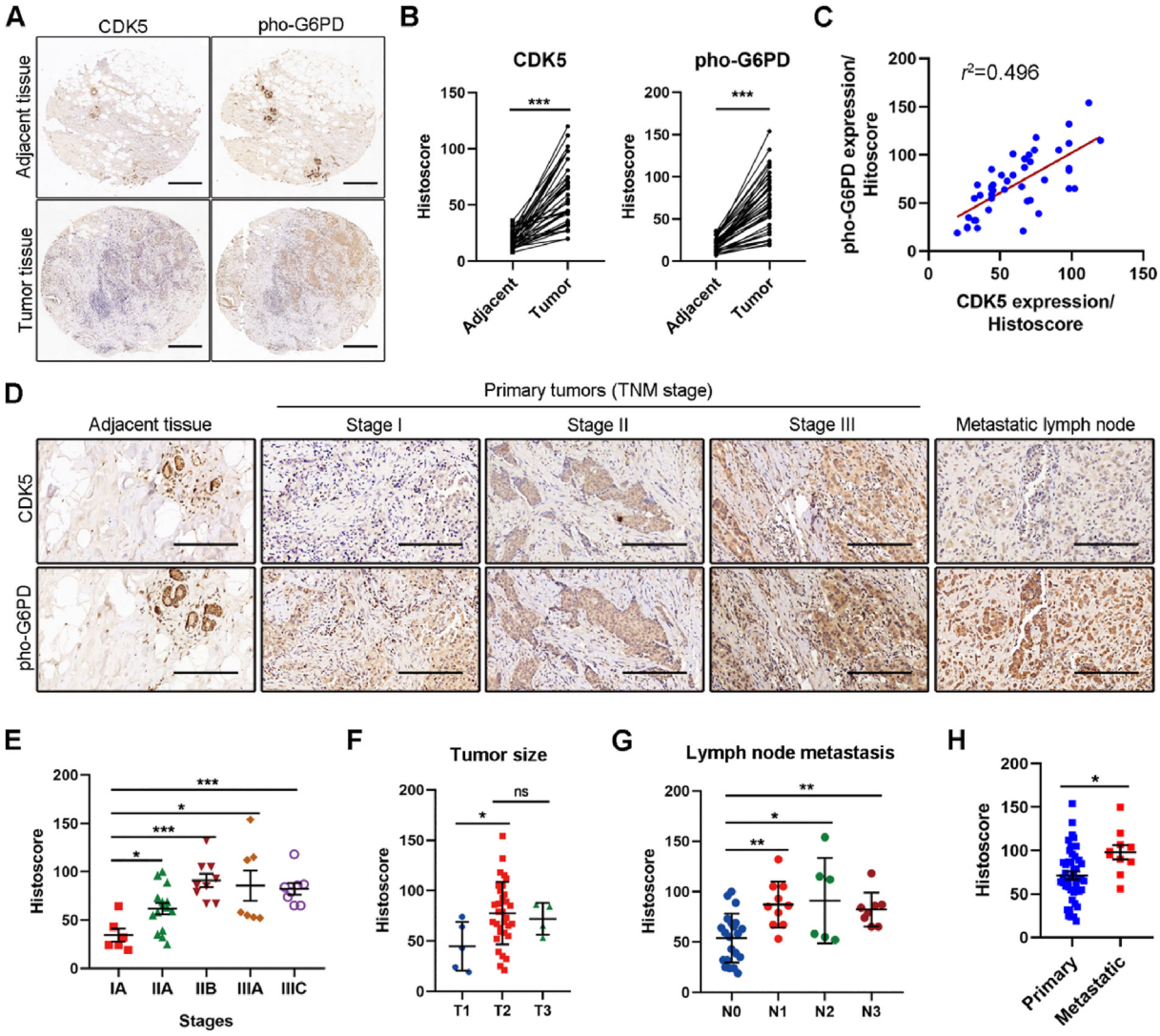

Figure 6 G6PD phosphorylation is implicated in human BC development. (A) Immunohistochemistry detection of G6PD phosphorylation at Thr-91 site, as well as CDK5, in tissue microarrays. Representative IHC images of G6PD phosphorylation, and CDK5 expression in human BC tumor tissues and paired adjacent normal tissues ($n = 45$). Scale bar = 500 μm. (B) Histoscores for G6PD phosphorylation, and CDK5 expression are summarized. (C) Correlation of CDK5 expression and G6PD phosphorylation (Pearson's correlation coefficient R was shown). (D, E) Representative IHC images of CDK5 expression, and G6PD phosphorylation at Thr-91 site in tumor tissues within different stages (D). Histoscores for each specimen are summarized according to TNM stages (E) (IA, $n = 6$; IIA, $n = 15$; IIB, $n = 9$; IIIA, $n = 7$; IIIC, $n = 8$). Scale bar = 100 μm. (F–H) The level of G6PD phosphorylation at Thr-91 site in tumor tissues with different tumor sizes (T1, $n = 7$; T2, $n = 34$; T3, $n = 4$) (F) or different percentages of lymph node metastasis (N0, $n = 21$; N1, $n = 10$; N2, $n = 6$; N3, $n = 8$) (G) were semi-quantitated by Histoscore. G6PD phosphorylation level was also detected in primary tumors and metastatic tumors ($n = 10$) (H). Data are present as mean ± SEM. Statistical significance was calculated using the student's *t*-test (A) and one-way ANOVA (C, D). ns, not significant, $^{*}P < 0.05$; $^{**}P < 0.01$; $^{***}P < 0.001$.

CDK5-induced phosphorylation of G6PD at the T91 site in BC cells during oxidative stress. Since active G6PD exists in a dimer-tetramer equilibrium but not as a monomer[35], we determined whether CDK5-mediated phosphorylation affected G6PD assembly. As shown in Fig. 4L, CDK5 inhibition and G6PD suppression remarkably promoted the dissociation of active G6PD dimers into inactive monomers, which was blocked by T91E mutation (Fig. 4M). Interestingly, G6PD-T91E, rather than G6PD-T91D, maintained G6PD active dimeric form, even in the presence of CDK5 inhibitor and G6PD inhibitor. Generally, these findings imply that CDK5-mediated phosphorylation at Thr-91 of G6PD enhanced its catalytic activity, possibly by stabilizing the G6PD homodimer.

These results reveal that Thr-91 was the target for CDK5-induced G6PD phosphorylation, which was pivotal for G6PD inducible activation and redox homeostasis under oxidative stress.

3.5. G6PD phosphorylation promotes tumor growth and lung metastasis of BC

Next, we investigated the influence of G6PD phosphorylation at the Thr-91 site on BC development *in vivo*. To accomplish this, we

established a xenograft mouse model by implanting MDA-MB-231 cells that overexpressed either WT G6PD (WT-OE) or T91A-mutated G6PD (T91A-OE) in opposite flanks of the same mouse as shown in Fig. 5A. Although the growth rate of T91A-OE cells was unaltered in comparison with that of WT-OE cells *in vitro* (Supporting Information Fig. S8A), T91A mutation significantly suppressed tumor growth *in vivo* (Fig. 5B and C). These results indicate that interruption of G6PD phosphorylation exhibited potential anticancer activity.

Similar to glucose deficiency, matrix detachment elicits oxidative stress[25], evidenced by elevated ROS production (Fig. S8B), which results in anoikis[36]. Developing anoikis resistance is critical for tumor cells to survive in circulation and form metastases[37]. *In vitro* assays revealed that CDK5-mediated G6PD phosphorylation induced colony formation in soft agar (Fig. S8C) due partly to elevated ROS detoxification capacity (Fig. S8D). Moreover, apoptotic assays confirmed that phosphorylated G6PD at the Thr-91 site promoted resistance to anoikis (Fig. S8E). For *in vivo* assay, WT-OE or T91A-OE cells were injected into the tail vein of nude mice (Fig. 5D), as described[25]. Pulmonary metastasis was assessed by *in vivo* quantitative bioluminescence imaging. As shown in Fig. 5D, WT-OE cells formed remarkably excessive lung metastases in comparison with T91A-OE cells. Hematoxylin and eosin staining of dissected lungs demonstrated the presence of more metastasis nodules in the WT-OE group in comparison with the T91A-OE group (Fig. 5E). Similarly, the same results were observed in tumor-bearing mice formed by transgenic MDA-MB-231 cell lines with G6PD T91 site-mutation (G6PD-WT, G6PD-T91A, G6PD-T91D and G6PD-T91E) (Fig. 5F and G, Fig. S8F and S8G). Altogether, our results demonstrate that CDK5-mediated G6PD phosphorylation at Thr-91 was critical for BC progression and metastasis.

3.6. *G6PD phosphorylation is implicated in human BC development*

Next, we turned to human BC specimens to address the importance of our findings in clinical samples. We generated a tissue microarray (TMA) composed of 45 paired adjacent-normal breast tissues and tumor tissues at various stages (IA: 6 cases; IIA: 15 cases; IIB: 9 cases; IIIA: 7 cases; IIIC: 8 cases). Next, the TMA was subjected to IHC by applying polyclonal antibodies to detect G6PD phosphorylation and applying polyclonal antibodies to detect G6PD phosphorylation and CDK5 expression. The intensity of each sample was quantified in a blind manner based on Histoscore. As shown in Fig. 6A, the CDK5 and phosphorylated G6PD levels in cancer tissues were much higher than in adjacent noncancerous breast tissues (Fig. 6A and B). CDK5 expression was tightly correlated with G6PD phosphorylation in clinical specimens (Fig. 6C), strengthening the conclusion that CDK5-mediated G6PD phosphorylation at the T91 site. Moreover, CDK5 and the G6PD phosphorylation levels were also elevated in advanced-stage tumor tissues (Fig. 6D and E). G6PD phosphorylation was dramatically evoked in tumors with large size (T2 and T3, Fig. 6F), primary tumors with lymph node metastasis (N1, N2, and N3, Fig. 6G), as well as metastatic tumors (Fig. 6H), which was consistent with the role of G6PD phosphorylation in limiting ROS and promoting the survival and metastasis of tumor cells during tumor development, as demonstrated in our mouse model (Fig. 5). These results reveal that G6PD phosphorylation at Thr-91 site occurs primarily in tumor tissues, rather than in normal tissues and it is closely associated with human BC development. Interestingly, we observed that CDK5-induced G6PD phosphorylation widely occurred in BC cell lines (Supporting Information Fig. S9). These data highlight CDK5-induced G6PD phosphorylation as a potential and promising target for BC therapy.

3.7. *Pharmacological inhibition of G6PD phosphorylation synergistically enhances conventional anticancer therapeutic efficacy in BC*

Given that oxidative stress defense programs are known to mediate therapy resistance, as many anticancer treatments cause cellular redox perturbation to induce cell death[38], we speculated that inhibition of CDK5-mediated G6PD phosphorylation might be an effective adjuvant therapy to enhance sensitization of cancer cells to ROS-inducing anticancer therapy. We applied several ROS-based therapeutic agents for further analysis to test this hypothesis. These included 5-fluorouracil (5-Fu)[39], paclitaxel[40], 5-azacytosine[41], olaparib[42], and berberine[43]. As shown in Fig. 7A, the intracellular ROS level was increased in MDA-MB-231 cells after treatment with these anticancer agents. Meanwhile, CDK5-mediated phosphorylation of G6PD at Thr-91 was induced in response to these anticancer treatments, particularly Olaparib treatment (Supporting Information Fig. S10A). These results prompted us to focus our subsequent *in vivo* analyses on Olaparib. Furthermore, T91A mutation significantly increased cell death in response to Olaparib and other treatments (Fig. 7B, Fig. S10B−S10D). CDK5-D144N (dead mutation) also sensitized BC cells to therapeutic agents (Fig. S10E). These observations indicated that CDK5-mediated G6PD phosphorylation was crucial for the adaptation of cancer cells to ROS-based anticancer therapies.

Next, we aimed to investigate the anti-tumoral activity of the combined therapeutic strategy by using CDK5 inhibitors and olaparib. In agreement with the biological effects triggered by T91A mutation observed previously, CDK5 inhibitors sensitized MDA-MB-231 cells to olaparib (Fig. 7C), due partly to enhanced DNA damage (Fig. 7D). As expected, G6PD phosphorylation at Thr-91 was notably abrogated in MDA-MB-231 cells after CDK5 inhibitors when combined with olaparib (Fig. 7D). However, little cytotoxicity was observed in normal HEK293 cells (Fig. S10F and S10G). The main reason might be that CDK5-induced phosphorylation of G6PD was more likely to be employed by tumor cells rather than normal cells (Fig. S9A and S9H).

Finally, we investigated whether inhibiting G6PD phosphorylation enhanced the therapeutic effects of Olaparib on BC *in vivo*. To this end, a xenograft mouse model was established as mentioned above, and the mice were subsequently injected with Olaparib (10 mg/kg) or CDK5 inhibitors (Rosc, 2 mg/kg; GFB-12811, 5 mg/kg), singly or in combination, on Days 7, 11, 15, 19, 23 and 27, post tumor implantation. As expected, combinatorial use of CDK5 inhibitors with Olaparib strongly inhibited tumor growth (Fig. 7E and F), and mice that received this treatment showed no alteration in body weight (Fig. S10I). For further confirmation, tumor tissues were systemically analyzed by IHC to assess proliferation, apoptosis, and DNA damage. As shown in Fig. 7G, administration of CDK5 inhibitors dramatically enhanced Olaparib-induced DNA damage, characterized by elevated gH2AX expression. Moreover, combinatorial treatments showed significant induction of persistent apoptosis, as demonstrated by active caspase 3 and TUNEL assay (Fig. 7G). Additionally, treatment with CDK5 inhibitors or olaparib, individually or in combination, had a slight inhibitory effect on the proliferation of tumor cells, defined by Ki67 expression (Fig. 7G). The antitumoral activity of this combined therapeutic strategy was also observed in MCF-7-bearing mice (Fig. S10J and S10K).

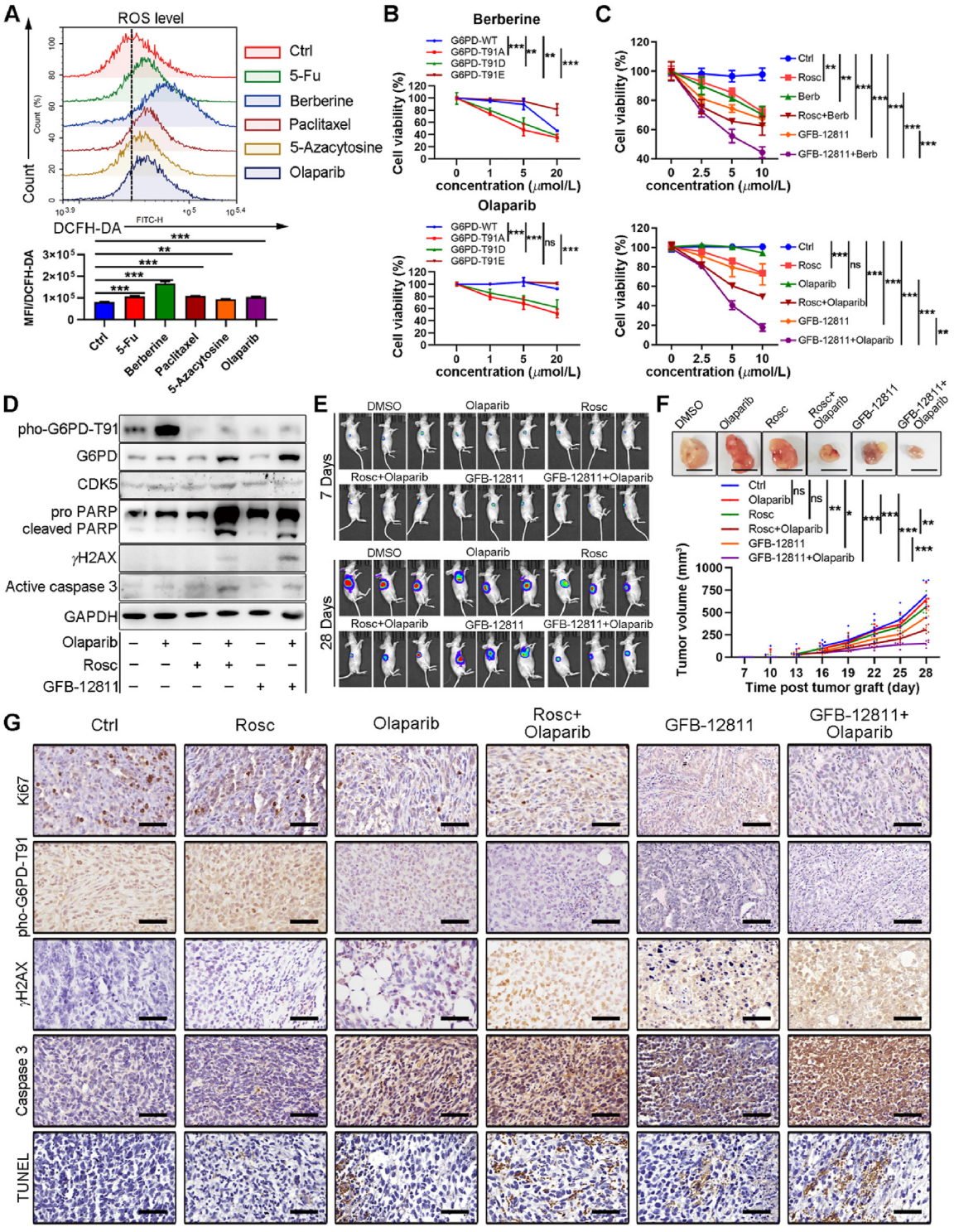

Figure 7 Pharmacological inhibition of G6PD phosphorylation synergistically enhances conventional anticancer therapeutic efficacy in BC. (A) MDA-MB-231 cells were treated with conventional anticancer agents as indicated. Flow cytometric analysis of intracellular ROS levels (Top) and MFI was summarized (bottom). (B) Transgenic MDA-MB-231 cells with G6PD T91 site mutation were treated with different concentrations of Berberine (top) and Olaparib (bottom) for 24 h. Cell viability was determined by using CCK-8 assay. (C) MDA-MB-231 cells were incubated with CDK5 inhibitor (CDK5, or GFB-12811) and Berb (or Olaparib), individually or in combination at the indicated concentration for 24 h. Cell viability was examined by CCK-8. (D) Cells from (C) were harvested and subjected to immunoblotting for analysis of the expression of phosphorylated G6PD at Thr-91 site, G6PD, CDK5, apoptosis-related pro-/cleaved-PARP, active caspase-3, as well as γH2AX. (E, F) *In vivo* analysis of the therapeutic effects of CDK5 inhibitor (Rosc, or GFB-12811) with/without Olaparib in the xenograft mouse model ($n = 6$). Representative bioluminescence images of xenograft mice on Days 7 and 28 after tumor implantation (E). Representative photographs of tumor tissues isolated at the end of the experiment. Scale bar = 1 cm. (F, top). Mean tumor volume was recorded at the indicated times (F, bottom). (G)

Taken together, these results illustrate that interrupting the CDK5/pho-G6PD axis synergistically enhanced the therapeutic effect of olaparib in HR-proficient BC cells. Furthermore, these findings demonstrate that interrupting the CDK5/pho-G6PD axis is a potential promising adjuvant for ROS-based anticancer therapy in BC patients.

4. Discussion

The regulation of redox homeostasis is a fundamental requirement for normal cellular functioning and survival. To cope with excessive ROS and maintain redox homeostasis, tumor cells have developed sophisticated antioxidant adaptation strategies, including metabolic reprogramming and activation of pro-oncogenic signaling pathways. In this study, we discovered that G6PD is modulated by CDK5-mediated Thr-91 phosphorylation, which enhances its catalytic activity and protects BC cells from oxidative stress-induced cell death. Inhibition of G6PD phosphorylation suppresses tumor growth and metastatic progression while sensitizing BC cells to conventional ROS-based anticancer agents. Most importantly, CDK5-induced G6PD phosphorylation occurs predominantly in tumor tissues, positively correlated with human BC progression. These findings reveal the mechanism by which cancer cells adapt to oxidative stress and a unique vulnerability of BC.

Oxidative stress is exerted mainly by intracellular ROS accumulates due to an imbalance between ROS generation and elimination. Despite their relatively strong antioxidant capacity, cancer cells exhibit higher ROS levels than normal cells[44]. This characteristic offers a rational therapeutic strategy because cancer cells might be more sensitive than normal cells to agents that cause further accumulation of ROS. Therefore, drugs used to increase ROS production have been put into clinical use for cancer patients[45]. Nonetheless, cancer cells can adapt to drug-induced oxidative stress by enhancing their antioxidant capacity, resulting in elevated resistance to chemotherapeutic drugs[46]. We found that inhibition of G6PD reduced the antioxidant capacity of BC cells, which would be expected to diminish multidrug resistance. Similar results have been reported in several types of cancer, including colorectal cancer[47], B-lineage lymphoid malignancies[48], and lung carcinoma[49]. Thus, targeting cancer cells' enhanced antioxidant defense mechanisms may provide promising strategies to impair tumor development and enhance the effects of conventional anticancer therapies.

5. Conclusions

G6PD has been identified as a promising target in cancer therapy because of its function in maintaining redox balance. We revealed that CDK5-mediated G6PD phosphorylation enhanced G6PD activity and protected BC cells against ROS-induced cell death, whereas suppressing G6PD phosphorylation impaired tumor growth and abrogated metastatic progression. Indeed, preclinical studies report that G6PD inhibitors, including 6-AN, DHEA[50], and natural products (catechin gallates[51], and rosmarinic acid[52]), exhibit therapeutic potential. However, their clinical use is limited by high oral doses, conversion of DHEA into active androgens, and on-target off-tumor toxicity of 6-AN at neurons[7]. Thus, novel strategies that modulate G6PD activity in a tumor-specific and enzyme-specific manner will facilitate the development of potent G6PD inhibitors. In this study, we discovered that CDK5-mediated threonine phosphorylation at G6PD Thr-91 is critical for G6PD activation[3], while it has little effect on basal activity. Moreover, CDK5-mediated G6PD phosphorylation predominantly occurs in tumor tissues rather than adjacent normal tissues, making it a promising tumor-specific target for cancer therapy. The regulatory mechanism of CDK5-mediated G6PD phosphorylation, reported here for the first time, represents an avenue for the development of applicable strategies to modulate G6PD activation. We found that pharmacological inhibition of G6PD phosphorylation at Thr-91 specifically attenuated the increase of G6PD activity induced by oxidative stress, which sensitized BC cells to ROS inducers *in vitro* and *in vivo*. Importantly, impairment of antioxidant defense *via* inhibition of G6PD phosphorylation synergistically enhanced the therapeutic efficacy of Olaparib against BC, while this combinatorial treatment produced limited cytotoxicity in normal cells (Fig. S6C). These results suggest that therapies targeting CDK5-mediated G6PD phosphorylation could serve as effective adjuvants for ROS-based treatment of BC patients.

Acknowledgments

This work was supported by grants from the Natural Science Foundation of Jiangsu Province (BK20222009, China), the National Natural Science Foundation of China (32341005), National Natural Science Foundation of China-Youth Program (32300762, China), Guangdong Basic and Applied Basic Research Foundation (2021B1515120016, China), the Key Research and the Nature Science Foundation of Jiangsu Province (BK20210027, China), and the Jiangsu Innovative and Enterpreneurial Talent Programme (JSSCBS20211488, China).

Author contributions

Yuncheng Bei: Writing − original draft, Methodology, Investigation, Funding acquisition, Formal analysis, Data curation. Sijie Wang: Software, Methodology, Investigation. Rui Wang: Visualization, Resources, Data curation. Owais Ahmad: Writing − review & editing, Writing − original draft, Software. Meng Jia: Resources. Pengju Yao: Software, Methodology, Investigation. Jianguo Ji: Supervision, Project administration, Funding acquisition. Pingping Shen: Writing − review & editing, Supervision, Project administration, Funding acquisition, Conceptualization.

Conflicts of interest

The authors declare no conflicts of interest.

Appendix A. Supporting information

Supporting information to this article can be found online at https://doi.org/10.1016/j.apsb.2024.12.019.

Representative IHC images for detection of Ki-67, G6PD phosphorylation, and γH2AX in tumor tissues isolated from mice (E). Apoptosis was detected by IHC analysis of active caspase-3 and TUNEL assay. Scale bar = 50 μm. Data are presented as mean ± SEM. Statistical significance was calculated using the two-way ANOVA (B−E), and one-way ANOVA (F). ns, not significant, $*P < 0.05$; $**P < 0.01$; $***P < 0.001$.

References

1. Hanahan D, Weinberg Robert A. Hallmarks of cancer: the next generation. *Cell* 2011;**144**:646−74.
2. de Mas IM, Aguilar E, Jayaraman A, Polat IH, Martin-Bernabe A, Bharat R, et al. Cancer cell metabolism as new targets for novel designed therapies. *Future Med Chem* 2014;**6**:1791−810.
3. Patra KC, Hay N. The pentose phosphate pathway and cancer. *Trends Biochem Sci* 2014;**39**:347−54.
4. Zhang L, Ye B, Chen Z, Chen ZS. Progress in the studies on the molecular mechanisms associated with multidrug resistance in cancers. *Acta Pharm Sin B* 2023;**13**:982−97.
5. Cho ES, Cha YH, Kim HS, Kim NH, Yook JI. The pentose phosphate pathway as a potential target for cancer therapy. *Biomol Ther* 2018;**26**:29−38.
6. Wang J, Yuan W, Chen Z, Wu S, Chen J, Ge J, et al. Overexpression of G6PD is associated with poor clinical outcome in gastric cancer. *Tumor Biol* 2012;**33**:95−101.
7. Zhang C, Zhang Z, Zhu Y, Qin S. Glucose-6-phosphate dehydrogenase: a biomarker and potential therapeutic target for cancer. *Anticancer Agents Med Chem* 2014;**14**:280−9.
8. Ratko TA, Detrisac CJ, Mehta RG, Kelloff GJ, Moon RC. Inhibition of rat mammary-gland chemical carcinogenesis by dietary dehydroepiandrosterone or a fluorinated analog of dehydroepiandrosterone. *Cancer Res* 1991;**51**:481−6.
9. Rao KVN, Johnson WD, Bosland MC, Lubet RA, Steele VE, Kelloff GJ, et al. Chemoprevention of rat prostate carcinogenesis by early and delayed administration of dehydroepiandrosterone. *Cancer Res* 1999;**59**:3084−9.
10. Inano H, Ishiiohba H, Suzuki K, Yamanouchi H, Onoda M, Wakabayashi K. Chemoprevention by dietary dehydroepiandrosterone against promotion/progression phase of radiation-induced mammary tumorigenesis in rats. *J Steroid Biochem* 1995;**54**:47−53.
11. Gessner T, Vaughan LA, Beehler BC, Bartels CJ, Baker RM. Elevated pentose cycle and glucuronyltransferase in daunorubicin-resistant P388 cells. *Cancer Res* 1990;**50**:3921−7.
12. Polimeni M, Voena C, Kopecka J, Riganti C, Pescarmona G, Bosia A, et al. Modulation of doxorubicin resistance by the glucose-6-phosphate dehydrogenase activity. *Biochem J* 2011;**439**:141−9.
13. Pozo K, Bibb JA. The emerging role of Cdk5 in cancer. *Trends Cancer* 2016;**2**:606−18.
14. Liu JL, Wang XY, Huang BX, Zhu F, Zhang RG, Wu G. Expression of CDK5/p35 in resected patients with non-small cell lung cancer: relation to prognosis. *Med Oncol* 2011;**28**:673−8.
15. Catania A, Urban S, Yan E, Hao CH, Barron G, Allalunis-Turner J. Expression and localization of cyclin-dependent kinase 5 in apoptotic human glioma cells. *Neuro Oncol* 2001;**3**:89−98.
16. Bei Y, Cheng N, Chen T, Shu Y, Yang Y, Yang N, et al. CDK5 inhibition abrogates TNBC stem-cell property and enhances anti-PD-1 therapy. *Adv Sci* 2020;**7**:2001417−32.
17. Daniels MH, Malojcic G, Clugston SL, Williams B, Coeffet-Le Gal M, Pan-Zhou XR, et al. Discovery and optimization of highly selective inhibitors of CDK5. *J Med Chem* 2022;**65**:3575−96.
18. Berkers CR, Maddocks ODK, Cheung EC, Mor I, Vousden KH. Metabolic regulation by p53 family members. *Cell Metab* 2013;**18**:617−33.
19. Zhao SM, Lin Y, Xu W, Jiang WQ, Zha ZY, Wang P, et al. Glioma-derived mutations in IDH1 dominantly inhibit IDH1 catalytic activity and induce HIF-1 alpha. *Science* 2009;**324**:261−5.
20. Gelman SJ, Naser F, Mahieu NG, McKenzie LD, Dunn GP, Chheda MG, et al. Consumption of NADPH for 2-HG synthesis increases pentose phosphate pathway flux and sensitizes cells to oxidative stress. *Cell Rep* 2018;**22**:512−22.
21. Li ML, Lu Y, Li YK, Tong LF, Gu XC, Meng J, et al. Transketolase deficiency protects the liver from DNA damage by increasing levels of ribose 5-phosphate and nucleotides. *Cancer Res* 2019;**79**:3689−701.
22. Malhotra JD, Miao H, Zhang K, Wolfson A, Pennathur S, Pipe SW, et al. Antioxidants reduce endoplasmic reticulum stress and improve protein secretion. *Proc Natl Acad Sci U S A* 2008;**105**:18525−30.
23. Sosa V, Moline T, Somoza R, Paciucci R, Kondoh H, Me LL. Oxidative stress and cancer: an overview. *Ageing Res Rev* 2013;**12**:376−90.
24. Klinman E, Holzbaur Erika LF. Stress-induced CDK5 activation disrupts axonal transport *via* Lis1/Ndel1/Dynein. *Cell Rep* 2015;**12**:462−73.
25. Lu YX, Ju HQ, Liu ZX, Chen DL, Wang Y, Zhao Q, et al. ME1 regulates NADPH homeostasis to promote gastric cancer growth and metastasis. *Cancer Res* 2018;**78**:1972.
26. Sena LA, Chandel NS. Physiological roles of mitochondrial reactive oxygen species. *Mol Cell* 2012;**48**:158−67.
27. Meng Q, Zhang Y, Hao S, Sun H, Liu B, Zhou H, et al. Recent findings in the regulation of G6PD and its role in diseases. *Front Pharmacol* 2022;**13**:932154−66.
28. Yang N, Wang Y, Tian Q, Wang Q, Lu Y, Sun L, et al. Blockage of PPARγ T166 phosphorylation enhances the inducibility of beige adipocytes and improves metabolic dysfunctions. *Cell Death Differ* 2023;**30**:766−78.
29. Kim C, Yun N, Lee J, Youdim MBH, Ju C, Kim WK, et al. Phosphorylation of CHIP at Ser20 by Cdk5 promotes tAIF-mediated neuronal death. *Cell Death Differ* 2016;**23**:333−46.
30. Xue Y, Zhou F, Zhu M, Ahmed K, Chen G, Yao X. GPS: a comprehensive www server for phosphorylation sites prediction. *Nucleic Acids Res* 2005;**33**:W184−7.
31. Guo L, Cai T, Chen K, Wang R, Wang J, Cui C, et al. Kindlin-2 regulates mesenchymal stem cell differentiation through control of YAP1/TAZ. *J Cell Biol* 2018;**217**:1431−51.
32. Dal Santo S, Stampfl H, Krasensky J, Kempa S, Gibon Y, Petutschnig E, et al. Stress-induced GSK3 regulates the redox stress response by phosphorylating glucose-6-phosphate dehydrogenase in Arabidopsis. *Plant Cell* 2012;**24**:3380−92.
33. Schastnaya E, Raguz Nakic Z, Gruber CH, Doubleday PF, Krishnan A, Johns NI, et al. Extensive regulation of enzyme activity by phosphorylation in *Escherichia coli*. *Nat Commun* 2021;**12**:5650−60.
34. Pearlman SM, Serber Z, Ferrell JE Jr. A mechanism for the evolution of phosphorylation sites. *Cell* 2011;**147**:934−46.
35. Au SWN, Gover S, Lam VMS, Adams MJ. Human glucose-6-phosphate dehydrogenase: the crystal structure reveals a structural $NADP^+$ molecule and provides insights into enzyme deficiency. *Structure* 2000;**8**:293−303.
36. Kim YN, Koo KH, Sung JY, Yun UJ, Kim H. Anoikis resistance: an essential prerequisite for tumor metastasis. *Int J Cell Biol* 2012;**2012**:306879−89.
37. Jin L, Chun J, Pan C, Kumar A, Zhang G, Ha Y, et al. The PLAG1−GDH1 axis promotes anoikis resistance and tumor metastasis through CamKK2−AMPK signaling in LKB1-deficient lung cancer. *Mol Cell* 2018;**69**:87−99.e7.
38. Gorrini C, Harris IS, Mak TW. Modulation of oxidative stress as an anticancer strategy. *Nat Rev Drug Discov* 2013;**12**:931−47.
39. Sun ZP, Zhang J, Shi LH, Zhang XR, Duan Y, Xu WF, et al. Aminopeptidase N inhibitor 4cc synergizes antitumor effects of 5-fluorouracil on human liver cancer cells through ROS-dependent CD13 inhibition. *Biomed Pharmacother* 2015;**76**:65−72.
40. Yang JC, Lu MC, Lee CL, Chen GY, Lin YY, Chang FR, et al. Selective targeting of breast cancer cells through ROS-mediated mechanisms potentiates the lethality of paclitaxel by a novel diterpene, gelomulide K. *Free Radic Bio Med* 2011;**51**:641−57.
41. Fandy TE, Jiemjit A, Thakar M, Rhoden P, Suarez L, Gore SD. Decitabine induces delayed reactive oxygen species (ROS) accumulation in leukemia cells and induces the expression of ROS generating enzymes. *Clin Cancer Res* 2014;**20**:1249−58.
42. Deben C, Lardon F, Wouters A, Op de Beeck K, Van den Bossche J, Jacobs J, et al. APR-246 (PRIMA-1(MET)) strongly synergizes with AZD2281 (olaparib) induced PARP inhibition to induce apoptosis in non-small cell lung cancer cell lines. *Cancer Lett* 2016;**375**:313−22.
43. Hur JM, Hyun MS, Lim SY, Lee WY, Kim D. The combination of berberine and irradiation enhances anti-cancer effects *via* activation of p38 MAPK pathway and ROS generation in human hepatoma cells. *J Cell Biochem* 2009;**107**:955−64.

44. Trachootham D, Alexandre J, Huang P. Targeting cancer cells by ROS-mediated mechanisms: a radical therapeutic approach?. *Nat Rev Drug Discov* 2009;**8**:579−91.
45. Chen Q, Li Q, Liang Y, Zu M, Chen N, Canup BSB, et al. Natural exosome-like nanovesicles from edible tea flowers suppress metastatic breast cancer *via* ROS generation and microbiota modulation. *Acta Pharm Sin B* 2022;**12**:907−23.
46. Traverso N, Ricciarelli R, Nitti M, Marengo B, Furfaro AL, Pronzato MA, et al. Role of glutathione in cancer progression and chemoresistance. *Oxid Med Cell Longev* 2013;**2013**:972913−22.
47. Ju HQ, Lu YX, Wu QN, Liu J, Zeng ZL, Mo HY, et al. Disrupting G6PD-mediated redox homeostasis enhances chemosensitivity in colorectal cancer. *Oncogene* 2017;**36**:6282−92.
48. McBrayer SK, Yarrington M, Qian J, Feng G, Shanmugam M, Gandhi V, et al. Integrative gene expression profiling reveals G6PD-mediated resistance to RNA-directed nucleoside analogues in B-cell neoplasms. *PLoS One* 2012;**7**:e41455-68.
49. Hong W, Cai P, Xu C, Cao D, Yu W, Zhao Z, et al. Inhibition of glucose-6-phosphate dehydrogenase reverses cisplatin resistance in lung cancer cells *via* the redox system. *Front Pharmacol* 2018;**9**:43−53.
50. Hamilton NM, Dawson M, Fairweather EE, Hamilton NS, Hitchin JR, James DI, et al. Novel steroid inhibitors of glucose 6-phosphate dehydrogenase. *J Med Chem* 2012;**55**:4431−45.
51. Shin ES, Park J, Shin JM, Cho D, Cho SY, Shin DW, et al. Catechin gallates are $NADP^+$-competitive inhibitors of glucose-6-phosphate dehydrogenase and other enzymes that employ $NADP^+$ as a coenzyme. *Bioorgan Med Chem* 2008;**16**:3580−6.
52. Tandogan B, Kuruuzum-Uz A, Sengezer C, Guvenalp Z, Demirezer LO, Ulusu NN. *In vitro* effects of rosmarinic acid on glutathione reductase and glucose 6-phosphate dehydrogenase. *Pharm Biol* 2011;**49**:587−94.
53. Bei Y, Chen J, Zhou F, Huang Y, Jiang N, Tan R, et al. BZ-26, a novel GW9662 derivate, attenuated inflammation by inhibiting the differentiation and activation of inflammatory macrophages. *Biomed Pharmacother* 2016;**84**:730−9.
54. Ma X, Wang L, Huang D, Li Y, Yang D, Li T, et al. Polo-like kinase 1 coordinates biosynthesis during cell cycle progression by directly activating pentose phosphate pathway. *Nat Commun* 2017;**8**:1506−20.
55. Bi J, Ichu TA, Zanca C, Yang H, Zhang W, Gu Y, et al. Oncogene amplification in growth factor signaling pathways renders cancers dependent on membrane lipid remodeling. *Cell Metab* 2019;**30**:525−538 e8.
56. An MX, Li S, Yao HB, Li C, Wang JM, Sun J, et al. BAG3 directly stabilizes Hexokinase 2 mRNA and promotes aerobic glycolysis in pancreatic cancer cells. *J Cell Biol* 2017;**216**:4091−105.